

Rotation and Macroturbulence in Metal-poor Field Red Giant and Red Horizontal Branch Stars

Bruce W. Carney¹

Department of Physics & Astronomy
University of North Carolina
Chapel Hill, NC 27599-3255
e-mail: bruce@unc.edu

David F. Gray

Department of Astronomy
University of Western Ontario
London, ON N6A 3K7, Canada
email:dfgray@uwo.ca

David Yong²

Department of Physics & Astronomy
University of North Carolina
Chapel Hill, NC 27599-3255
e-mail: yong@physics.unc.edu

David W. Latham

Harvard-Smithsonian Center for Astrophysics
60 Garden Street, Cambridge, MA 02138
e-mail: dlatham@cfa.harvard.edu

Nadine Manset & Rachel Zelman

Canada-France-Hawaii Telescope Corporation
65-1238 Mamalahoa Highway
Kamuela, HI 96743
email: manset@cfht.hawaii.edu; zelman@cfht.hawaii.edu

John B. Laird

Department of Physics & Astronomy
Bowling Green State University
Bowling Green, OH 43403
e-mail: laird@bgsu.edu

ABSTRACT

We report the results for rotational velocities, $V_{\text{rot}} \sin i$, and macroturbulence dispersions, ζ_{RT} , for 12 metal-poor field red giant branch (RGB) stars and 7 metal-poor field red horizontal branch (RHB) stars. The results are based on Fourier transform analyses of absorption line profiles from high-resolution ($R \approx 120,000$), high-S/N (≈ 215 per pixel; ≈ 345 per resolution element) spectra obtained with the Gecko spectrograph at CFHT. The stars were selected from the studies of 20 RHB and 116 RGB stars from Carney et al. (2003, 2007), based primarily on larger-than-average line broadening values. We find that ζ_{RT} values for the metal-poor RGB stars are very similar to those for metal-rich disk giants studied earlier by Gray and his collaborators. Six of the RGB stars have small rotational values, less than 2.0 km s^{-1} , while five show significant rotation/enhanced line broadening, over 3 km s^{-1} . We confirm the rapid rotation rate for RHB star HD 195636, found earlier by Preston (1997). This star's rotation is comparable to that of the fastest known rotating blue horizontal branch (BHB) stars, when allowance is made for differences in radii and moments of inertia. The other six RHB stars have somewhat lower rotation but show a trend to higher values at higher temperatures (lower radii). Comparing our results with those for BHB stars from Kinman et al. (2000), we find that the fraction of rapidly rotating RHB stars is somewhat lower than is found among BHB stars. The number of rapidly rotating RHB stars is also smaller than we would have expected from the observed rotation of the RGB stars. We devise two empirical methods to translate the line broadening results obtained by Carney et al. (2003, 2007) into $V_{\text{rot}} \sin i$ for all the RGB and RHB stars they studied. Binning the RGB stars by luminosity, we find that most metal-poor field RGB stars show no detectable sign, on average, of rotation, which is not surprising given the stars' large radii. However, the most luminous stars, with $M_V \leq -1.5$, do show net rotation, with mean values of 2 to 4 km

¹Based on observations obtained at the Canada-France-Hawaii Telescope (CFHT) which is operated by the National Research Council of Canada, the Institut National des Sciences de l'Univers of the Centre National de la Recherche Scientifique de France, and the University of Hawaii.

²Mt. Stromlo Observatory
Cotter Road, Weston Creek
Canberra, ACT 72611, Australia
email: yong@mso.anu.edu.au

s^{-1} , depending on the algorithm employed, and also show signs of radial velocity jitter and mass loss. This “rotation” may in fact prove to be due to other line broadening effects, such as shock waves or pulsation.

Subject headings: stars: binaries: spectroscopic; kinematics; planetary systems; Population II; rotation; Galaxy: halo

1. INTRODUCTION

In previous papers (Carney et al. 2003, Carney et al. 2007; hereafter C2003, C2007) we reported on radial velocities and line broadenings for 136 metal-poor field red giant branch (RGB) and red horizontal branch (RHB) stars, based on 2413 high-resolution, low-S/N spectra. One of the more intriguing results was that the more luminous red giants, as well as many of their evolutionary progeny, red horizontal branch stars, showed significant line broadening. Interpreting the enhanced line broadening as rotation, C2003 explored the possibility that it might have arisen from absorption of one (or more) jovian mass planets that were engulfed only as the red giants swelled to large enough radii.

C2003 suggested several follow-up studies. First, the sample size should be expanded, and C2007 presented the results for 45 stars to complement the original 91-star sample of C2003. Second, high-precision radial velocity monitoring of metal-poor dwarfs and subgiants should be undertaken to explore the frequency of jovian-mass planets with orbital periods of order one year, corresponding to aphelion distances comparable to the maximum radial size of metal-poor RGB stars. The initial results of such a study have been reported (Sozzetti et al. 2006), and it appears that such planetary companions are not sufficiently common to explain the modest frequency of significant line broadening among the most luminous metal-poor red giants.

This paper explores the separate contributions of rotation and macroturbulence, based on a selected subsample of stars studied by C2003 and C2007. For example, if macroturbulence is a strong function of luminosity, the enhanced line broadenings found by C2003 and C2007 among the field red giants might be explained. If macroturbulence is a strong function of temperature, perhaps the line broadening seen in some of the red horizontal branch stars could also be explained. But if rotation is the cause of the enhanced line broadening among the stars with the largest radii, some new explanations must be sought.

To test these hypotheses, we decided to exploit methods developed by Gray (1982), whereby line profiles measured using very high-resolution, high-S/N spectra could be

analyzed via Fourier transform methods to distinguish the contributions of rotation and macroturbulence.

2. PROGRAM DESCRIPTION

The Fourier transform method requires very high-resolution and high-S/N spectra. The Gecko spectrograph on the Canada-France-Hawaii Telescope (CFHT) was deemed to be an ideal instrument for our work, but the wavelength coverage is quite limited. We therefore computed a grid of model atmospheres covering the stellar parameters appropriate to our field RHB and RGB stars, using ATLAS9. We then computed synthetic spectra using R. L. Kurucz's code SYNTHE. We sought wavelength regions that had a significant number of uncrowded absorption lines. The lines must be reasonably strong, but not saturated since pressure-broadened line wings render the lines less useful. We determined that for the red horizontal branch stars, the optimal wavelength region should be centered at 5430 Å, while for the red giants, the central region should be 6150 Å. Figure 1 shows the spectra for one of the RGB and one of the RHB stars.

Because of the requirement for high-S/N, and limited available observing time, we had to choose our targets carefully. Of course we selected a number of RHB and RGB stars with significant line broadening. We also elected to observe a few stars with smaller line broadening, partly as a test of the line broadening derived from the lower-resolution ($R \approx 32,000$) CfA spectra. Further, if the line broadening is due to rotation, we assume that the less-broadened stellar spectra might reflect nearly pole-on inclinations, so that we could explore macroturbulence more carefully.

Our observations were obtained in two runs with the CFHT, and to check the consistency of our results, we observed HD 29574 during both. We also felt a need to compare our results with the extensive studies of disk stars completed earlier by Gray (1982, 1984), Gray & Toner (1986, 1987), and Gray & Pallavicini (1989). We therefore included η Ser (HR 6869) in our program, which had been studied previously by Gray & Pallavicini (1989).

3. OBSERVATIONS

We used the Gecko spectrograph at the CFHT on two observing runs, in December 2004 and October 2006. We used the MIT2 detector, a thinned 2048×4096 chip with 15μ pixels. The read noise for this device is about 7.5 electrons, which was negligible given

the strong exposures. The gain setting was 1.2 electrons per ADU. Gecko was fiber-fed by CAFE (Baudrand & Vitry 2000) from the Cassegrain focus of the telescope. Fiber modal noise was suppressed by agitating the fiber continuously (Baudrand and Walker 2001).

The RGB stars were observed using order 9 and the 1521 filter. The single order on the detector at 6150 Å spans only about 90 Å, and the dispersion is about 1.47 Å mm⁻¹ (0.022 Å pixel⁻¹). The RHB stars were observed using order 10 and the 1510 filter, which covered 86 Å at a dispersion of 1.40 Å mm⁻¹, or about 0.021 Å pixel⁻¹. We measured the resolution using Th-Ar comparison lines, finding a typical resolving power of 120,000. Figure 2 shows 8 Å coverage in spectra of two red giant branch stars. The line depths are comparable, and it is (marginally) apparent that HD 3008 is broader lined than HD 23798, as the analyses of both the CfA and the CFHT spectra revealed.

Table 1 provides a log of our observations, including the exposure time in minutes, the heliocentric Julian date of mid-exposure, and the estimated signal-to-noise obtained *per pixel*. Each spectral resolution element covered about 2.3 pixels, so the S/N per resolution element is that given in Table 1 multiplied by a factor of about 1.5.

4. DERIVATION OF ROTATIONAL AND MACROTURBULENT VELOCITIES FOR CFHT PROGRAM STARS

Since the Doppler broadening of rotation and macroturbulence are comparable in size, it is necessary to push toward high Fourier frequencies in order to distinguish the subtle differences in shape they impress upon the spectral lines. This is why the high resolving power of the Gecko spectrograph was needed. But high resolving power alone is not sufficient because the amplitudes at high Fourier frequencies are small and often below the noise level. For this reason high signal-to-noise ratios are also needed. Most of our observations are of sufficient quality to fulfill these requirements and allow us to distinguish rotation from macroturbulence.

Individual line profiles were extracted and corrected for small blends when necessary. The Fourier analysis then proceeds in the usual way (Gray 2005) by first dividing out the transform of a thermal profile computed from a model photosphere. Effective temperatures, surface gravities, and metallicities were taken from C2003 and C2007. Treatment of the thermal profile is not overly critical since its width is considerably smaller than the observed line widths. When this step is completed for all the usable lines, an average of these ratios is taken. The final manipulation of the data is to divide out the transform of the instrumental profile. We took the profile of a narrow emission line in a thorium-argon comparison lamp

to be the instrumental profile. While we would have preferred using a narrower-line source, none was available. However, we expect no serious error to be introduced because the instrumental profile is many times narrower than the stellar lines. Since both the transforms of the thermal profile and the instrumental profile decline toward larger frequencies, division by them enhances the noise at the high frequencies. The transition to enhanced noise is fairly abrupt. Naturally, our analysis is restricted to Fourier frequencies below this transition.

The distribution of Doppler shifts from rotation and Radial-Tangential macroturbulence (Gray 2005) are computed by integrating over a model stellar disk on a sector-annulus format. A sector step of 0.5 degree was used and the annulus dimension was adjusted to be of comparable linear dimension. A limb darkening coefficient ($\epsilon = 0.7$) was used. Fourier transforms of these Doppler-shift distributions are compared with the observations, and the broadening parameters, $V_{\text{rot}} \sin i$ and ζ_{RT}^3 , are adjusted until the best match is obtained. The ratio of rotational to macroturbulence broadening, $V_{\text{rot}} \sin i / \zeta_{\text{RT}}$, is determined from the curvature and any sidelobe structure. The absolute scale of the velocities comes from the translational match on the logarithmic abscissa. In those cases where $V_{\text{rot}} \sin i$ is considerably smaller than ζ_{RT} , $V_{\text{rot}} \sin i$ will be poorly determined, and vice versa. We estimated the errors by altering the $V_{\text{rot}} \sin i$ and ζ_{RT} parameters by small amounts until obvious mismatch with the data occurs. Two examples of the final step are shown in Figure 3. HD 195636 is a rapid rotator, while HD 184266 has some rotation but larger macroturbulence. Table 2 summarizes the results of the Fourier analyses.

Our results appear to be consistent between the two observing runs, based on the very good agreement for the two sets of measurements of HD 29574. Further, our results for η Ser, $V_{\text{rot}} \sin i = 1.0 \pm 0.8 \text{ km s}^{-1}$ and $\zeta_{\text{RT}} = 4.1 \pm 0.5 \text{ km s}^{-1}$, agree very well with those obtained by Gray & Pallavicini (1989), 2.0 ± 0.5 and $4.0 \pm 0.5 \text{ km s}^{-1}$, respectively.

³ ζ_{RT} is the radial-tangential macroturbulence dispersion. It is not the Gaussian macroturbulent velocity, but is roughly 2.4 times larger (Gray 1978).

5. RESULTS

5.1. Radial Velocities

The radial velocities for each star reported in Table 1 were derived using **rvsao** (Kurtz & Mink 1998) running inside the IRAF⁴ environment. We compare our results with those reported in C2003 and C2007 (which therefore excludes η Ser). We do not include HD 218732 in the comparisons because it is a spectroscopic binary.

For the 11 stars not known to suffer velocity “jitter” (see C2003 and C2007 for a more complete discussion of this phenomenon), we find $\langle V_{\text{rad,CFHT}} - V_{\text{rad,CfA}} \rangle = +0.13 \pm 0.14$ km s⁻¹, with $\sigma = 0.46$ km s⁻¹. This agreement is very satisfactory. For the 8 other stars known to be subject to “jitter”, the mean difference is -0.71 ± 0.44 km s⁻¹, with $\sigma = 1.24$ km s⁻¹. Considering the velocity variations in these stars, this agreement is good.

5.2. A First Look at Rotational and Macroturbulent Velocities

Figure 4 distinguishes the RGB (filled circles) from the RHB stars (open circles) in the $V_{\text{rot}} \sin i$ vs. ζ_{RT} plane. Several points are apparent from the Figure.

First, much of the line broadening found by C2003 and C2007 for the most luminous red giants, with V_{broad} ⁵ values approaching 12 km s⁻¹, is due more to macroturbulence than to rotation, whose maximal value among the 12 RGB stars we have studied is only 5.5 km s⁻¹. The 12 RGB stars have $\langle V_{\text{broad,CfA}} \rangle = 8.1 \pm 0.6$ km s⁻¹ ($\sigma = 2.2$ km s⁻¹), but $\langle V_{\text{rot}} \sin i \rangle = 2.3 \pm 0.6$ km s⁻¹ ($\sigma = 1.9$ km s⁻¹), and $\langle \zeta_{\text{RT}} \rangle = 6.8 \pm 0.2$ km s⁻¹ ($\sigma = 0.7$ km s⁻¹).

Second, the macroturbulence levels are generally higher in the observed RHB stars than in the RGB stars, with $\langle \zeta_{\text{RT}} \rangle = 9.1 \pm 0.7$ ($\sigma = 1.8$ km s⁻¹). The RHB stars have higher gravities than the RGB stars, so we would be tempted to assume that macroturbulence increases at higher gravities, smaller radii, or lower luminosities, but the discussion in Section 6.2.2 reveals the opposite to be the case. This also conflicts with the findings of Gray (1982) and Gray & Pallavicini (1989), who found that lower gravity disk giants have

⁴IRAF (Image Reduction and Analysis Facility) is distributed by the National Optical Astronomy Observatories, which are operated by the Association of Universities for Research in Astronomy, Inc., under contract with the National Science Foundation.

⁵Note that C2003 refer to rotational velocities, $V_{\text{rot}} \sin i$, but which we prefer to call broadening velocities, V_{broad} .

higher values of ζ_{RT} . Therefore, temperature must play a significant role as well, as had been demonstrated earlier by Gray (1982) and by Gray & Toner (1986).

Third, rotation and macroturbulence play comparable roles in the line broadening of the observed RHB stars. Including the rapid rotator HD 195636, $\langle V_{\text{rot}} \sin i \rangle = 9.5 \pm 2.2 \text{ km s}^{-1}$ ($\sigma = 6.0 \text{ km s}^{-1}$). Excluding that star, $\langle V_{\text{rot}} \sin i \rangle = 7.4 \pm 0.9 \text{ km s}^{-1}$ ($\sigma = 2.3 \text{ km s}^{-1}$). These values are comparable to $\langle \zeta_{\text{RT}} \rangle$ for the observed RHB stars.

Fourth, the RHB stars show higher rotational velocities than the RGB stars, especially in the case of HD 195636, a star whose rapid rotation was noted first by Preston (1997). Since RHB stars represent some of the descendents of RGB stars, and since RHB stars have smaller radii, more rapid rotation is expected. But there is a discrepancy when the results are examined more closely. Taking simple means, we find that the 12 RGB stars have $\langle R \rangle = 68 R_{\odot}$, while the 7 RHB stars have $\langle R \rangle = 7.5 R_{\odot}$ ($7.2 R_{\odot}$ if we exclude HD 195636). We have been unable to find published moments of inertia of RGB and RHB stars, so we make the assumption that since the core masses and total masses of both classes of star are similar, then if the envelope density distributions are similar, the total moment of inertia will scale as the stellar radii. In this case, we expect the RHB stars to be rotating about nine times faster than the mean RGB rotation rate. The ratio is, in fact, 4.1, if we include HD 195636, and is 3.2 if we exclude it. While our RGB and RHB samples were selected with a bias in favor of larger line broadening, this does not alter our conclusion. In subsection 7.2.2. (see Table 5), we found that the mean V_{broad} value for the twenty most luminous red giants is 7.7 km s^{-1} , very similar to the 8.1 km s^{-1} for the RGB stars observed at CFHT. So the bias does not strongly affect the mean rotational value of the luminous red giants. The same is not true for the RHB stars, however. The seven RHB stars in Table 2 have $\langle V_{\text{broad}} \rangle = 13.4 \text{ km s}^{-1}$ (12.0 km s^{-1} if we exclude HD 195636), while the thirteen RHB stars not observed at CFHT have $\langle V_{\text{broad}} \rangle = 6.4 \text{ km s}^{-1}$. Correcting for the bias for the RHB sample will only lower their mean rotational velocities, increasing the magnitude of the discrepancy between the expected ratio of rotational velocities. What might cause the discrepancy? One possibility is the loss of angular momentum, perhaps by a vigorous stellar wind or pulsation at the most luminous final stages of RGB evolution. RHB stars have larger envelopes than BHB stars, so, presumably, RHB stars lost less mass during the RGB stage. But as we discuss in Section 7.1.3, it is not clear that the two classes of HB stars have significantly different net amounts of angular momentum. Finally, and this bears on discussions below, the rotation we have measured in the most luminous red giants may reflect a combination of rotation and some other effect, such as pulsation, that may also result in line broadening.

5.3. The Case of HD 195636

The rotation of HD 195636 is much higher than the other RHB stars. It is, however, not out of line with the maximal rotation seen in blue horizontal branch stars. We consider the BHB stars studied by Kinman et al. (2000), excluding BD+32 2188 because the radius derived from its $\log g$ value, $11.8 R_{\odot}$, suggests it is not a BHB star. Of the remaining 29 stars, two have $V_{\text{rot}} \sin i \approx 40 \text{ km s}^{-1}$, and estimated radii of about $3.3 R_{\odot}$. At the estimated radius of HD 195636, $\approx 9.1 R_{\odot}$, this would correspond to a rotational velocity of about 15 km s^{-1} , somewhat smaller than our derived value of 22 km s^{-1} . If these largest rotational velocities simply reflect stars with the most favorable viewing angles ($\sin i \approx 1$), this small sample suggests that there is no great difference between the maximum values of rotation in BHB and RHB stars.

In drawing attention to this star, Preston (1997) explored whether a close binary companion could have interacted tidally, producing such a high rotational velocity. Preston's observations had limited time coverage, but displayed no sign of radial velocity variability. C2003 reported 43 radial velocities covering 5086 days (13.9 years), and did not detect any radial velocity variability. Our additional radial velocity measure (Table 1) extends the time coverage to 8460 days (23.2 years), and the star has maintained the same radial velocity. We conclude that tidal locking in a binary system is not the source of the rapid rotation. Indeed, of the 20 RHB stars studied by C2003 and C2007, only one has proven to be a spectroscopic binary (HD 108317), and it has one of the smallest line broadening measures (C2003), with $V_{\text{broad,CfA}} = 5.1 \text{ km s}^{-1}$. Tidal locking does not explain the relatively high rotational velocities seen in some of our RHB stars.

6. ESTIMATION OF ROTATIONAL VELOCITIES & MACROTURBULENT DISPERSIONS FOR A LARGER SAMPLE OF STARS

We have obtained rotational velocities and macroturbulent dispersions for 7 of the 20 RHB stars studied by C2003 and C2007, and 12 of the 116 RGB stars. Further, those 12 RGB stars are all near the tip of the red giant branch. We believe we can extract rotational velocity estimates of the other 13 RHB and 104 RGB stars, at least in a statistical sense.

We use two basic approaches. In one case, we seek to identify a means whereby we can reliably estimate ζ_{RT} as a function of some parameter, such as absolute magnitude, gravity, or temperature, and then employ some algorithm to remove that contribution to the total line broadening determined using the CfA spectra. In the second case, we simply compare

the V_{broad} values determined from the CfA spectra with the rotational velocities obtained from the CFHT data. This essentially assumes that macroturbulence is either constant among our program stars or small in comparison with rotation.

In the first case, following Massarotti et al. (2007), C2007 found that

$$V_{\text{broad}} = [(V_{\text{rot}} \sin i)^2 + 0.95\zeta_{\text{RT}}^2]^{1/2}. \quad (1)$$

Figure 5 compares the results from this Equation using our CFHT data with those derived at CfA. It is important to recall that this is a purely empirical fit. It is not based on any deep physical understanding of the phenomena of rotation and macroturbulence. Indeed, it is hard to justify because ζ_{RT} does not behave as a Gaussian in broadening a stellar absorption line (Gray 2005). We employ the relation solely on the basis that it appears to provide a good fit to our data. The 0.95 coefficient was determined empirically by comparing the results given in Table 2 with the line broadening estimates from the CfA observations. Specifically, 0.95 was necessary to provide a negligible offset between $V_{\text{broad,CFHT}}$ and $V_{\text{broad,CfA}}$. The resultant scatter in the relation was only 1.1 km s^{-1} , and was even smaller, 0.9 km s^{-1} , for stars whose line broadenings were smaller than the resolution of the CfA spectra (8.5 km s^{-1}).

In the second case, we show in Figure 6 a second-order fit between the V_{broad} values derived from our CfA spectra with the $V_{\text{rot}} \sin i$ values from the much higher resolution and much higher S/N CFHT spectra. Filled circles are RGB stars, while open circles are RHB stars. The fit is remarkably good, with a scatter of only 1.5 km s^{-1} .

$$V_{\text{rot}} \sin i = -1.12 + 0.044V_{\text{broad}} + 0.0488V_{\text{broad}}^2 \quad (2)$$

Note that in both cases we have relied on both the RHB and the RGB stars to calibrate the relations. We will employ both methods to estimate $V_{\text{rot}} \sin i$ for all of our CfA program stars that were not observed at CFHT.

6.1. Macroturbulence Among the Red Horizontal Branch Stars

To make use of Equation 1, we need to have good estimates for the contribution of the macroturbulence to the total line broadening. Figure 7 summarizes our macroturbulence dispersions as a function of temperature and gravity. Let us focus first on the seven RHB stars at the lower left of the Figure. The stars have very similar luminosities and gravities, but have a respectable range in effective temperature, from about 5300 K to almost 6200 K. However, there is no obvious correlation between T_{eff} and ζ_{RT} . A weighted least squares fit

results in

$$\zeta_{\text{RT}} = -0.00158T_{\text{eff}} + 18.17, \quad (3)$$

with a correlation coefficient of only -0.28 . The scatter about this relation is 1.7 km s^{-1} , which is negligibly better than taking the mean value for all 7 stars, which, as noted above, results in $\langle \zeta_{\text{RT}} \rangle = 9.1 \pm 0.7 \text{ km s}^{-1}$, with $\sigma = 1.8 \text{ km s}^{-1}$. In Section 7.1, we return to this topic, finding an additional reason to doubt that a simple description of the behavior of ζ_{RT} can be applied to RHB stars. On the other hand, the RGB stars appear to be well-behaved, as we discuss below.

6.2. Expanding the Sample of Calibrating Red Giants

As we have pointed out, the red giant stars studied in this program tend to lie near the tip of the RGB, as may be seen in Figure 7. But the other 104 RGB stars in C2003 and C2007 have a much wider range of luminosities, temperatures, and gravities, and hence we require additional data. Since our results appear to be in good agreement with those obtained for the disk population giant η Ser, we explore now how the results for our metal-poor field red giants compare with results obtained earlier for metal-rich disk population field red giants.

6.2.1. Selection of Disk Stars

The behavior of macroturbulence and rotation of very old and very metal-poor halo stars merits comparisons with the values of younger and more metal-rich disk stars. We have assembled a sample of disk stars from the work of Gray (1982, 1984, 1989), Gray & Toner (1986, 1987), and Gray & Pallavicini (1989), who employed the same tools to determine $V_{\text{rot}} \sin i$ and ζ_{RT} from very high-resolution, very high S/N spectra, as employed here. Stars retained in the final comparisons with the halo giants had to satisfy several criteria.

First, we chose to exclude stars with spectral types earlier than G8. Nothing is lost thereby since our halo stars have temperatures cooler than this. The additional benefit is that the stars we employ are cooler than the transition in rotational velocities seen in giant stars with G spectral types (Gray 1989). Stars cooler than G0 to G3 III stars have significantly lower rotational velocities than warmer stars, presumably due to a rotational dynamo-generated magnetic brake.

We elected to retain only those stars with a consistently-applied photometric or high-

resolution spectroscopic approach to determinations of stellar parameters. We are fortunate that McWilliam (1990) undertook an extensive spectroscopic survey of metallicities of disk giants, and employed consistent photometric estimations of temperatures and gravities. Fortunately, many of the stars in the studies by Gray and his colleagues were also studied by McWilliam. We have adopted his photometric estimates of effective temperature and gravity, and his spectroscopic determinations of $[\text{Fe}/\text{H}]$. However, to avoid extending the comparisons of disk giants and halo giants to temperatures far beyond those of our available halo sample giant stars, we have retained only those stars in McWilliam (1990) with $T_{\text{eff}} \leq 5000$ K, in order to be consistent with the use of stars with spectral types of G8 and later.

Gray (1982) noted that the macroturbulence dispersions, ζ_{RT} , are double-valued for spectral classes G8 through K2, with weaker lines indicating larger values than stronger lines in the same star. We have adopted a straight average of the two sets of results because we are going to apply the ζ_{RT} results to the line broadenings, V_{broad} , determined from the CfA spectra (C2003, C2007). Those velocities, in turn, were determined from a match involving all lines, weak and strong, in a narrow wavelength region. Finally, we replaced ζ_{RT} values from Gray (1982) with the newer values presented by Gray (1989).

Absolute visual magnitudes were determined for all the disk stars using parallaxes from HIPPARCOS. Following McWilliam (1990), we assumed that most stars had zero interstellar absorption. For the stars for which McWilliam estimated A_V values (his Table 7), we adopted those values. We had to exclude γ^2 Leo because it does not have a measured V magnitude.

We adopted uncertainties for the determinations of $V_{\text{rot}} \sin i$ and ζ_{RT} given by Gray & Toner (1986, 1987), and by Gray (1989). Gray (1982) did not provide such estimates, so we conservatively adopted $\sigma(V_{\text{rot}}) = \sigma(\zeta_{\text{RT}}) = 1.0 \text{ km s}^{-1}$. For the stars from the work of Gray & Pallavicini (1989), we used only the ESO spectra and the lines in the $\lambda 6250$ domain, for which the errors were estimated to be $\pm 0.5 \text{ km s}^{-1}$. Table 3 summarizes the results for the 32 disk giants that satisfied the above criteria, although as discussed below, we chose to not use all of them in the final analyses.

6.2.2. Halo Giants vs. Disk Giants

In Figures 8 through 10 we compare the macroturbulent dispersions, ζ_{RT} , we have derived for the halo giants and results for disk giants discussed above. Open triangles are disk stars with luminosity classes Ib or II, open squares are disk stars with luminosity class

II-III, and open circles are disk giants of luminosity class III. The filled circles represent the halo giants observed at CFHT. Two significant results are apparent.

First, the Ib and II stars do not show a consistent trend. This should be expected, since these stars are generally descendents of massive stars, which do not undergo as much rotational braking while on the main sequence, nor even during their very brief spans as red supergiants or bright giants.

Second, with the exceptions of β Sge and λ Peg, the rest of the disk stars appear to follow the same trends as the older halo giants. If we discard the luminosity class Ib and II stars, as well as β Sge and λ Peg, and employ weighted least squares fits, we find:

$$\zeta_{\text{RT}} = -0.62M_V + 5.307, \quad (4)$$

with a scatter of only 0.7 km s^{-1} , and a correlation coefficient of -0.78 . If we consider the gravity, we find:

$$\zeta_{\text{RT}} = -0.80 \log g + 7.33. \quad (5)$$

In this case the scatter is only slightly greater, 0.8 km s^{-1} , and the correlation coefficient, $R = -0.72$, is likewise slightly inferior. Using effective temperature as the independent variable, we find:

$$\zeta_{\text{RT}} = 10.85T_{\text{eff}} - 6.54. \quad (6)$$

The scatter, 1.0 km s^{-1} , and the correlation coefficient, -0.59 , are a little worse than in the above two cases. While it is true that for a fixed age and metallicity, red giants obey monotonic relations between the three independent variables, M_V , $\log g$, and T_{eff} , when we mix in stars of different metallicities and ages, such correlations fail. Consider, for example, a metal-rich disk giant with $[\text{Fe}/\text{H}] = -0.27$, $[\alpha/\text{Fe}] = 0.0$, an age of 5 Gyrs, and $T_{\text{eff}} = 4000 \text{ K}$. According to the ‘‘Yale-Yonsei’’ isochrones (Yi et al. 2003; Demarque et al. 2004), such a star has $\log g = +1.29$ and $M_V = -0.77$. A typical halo giant with the same temperature, but with $[\text{Fe}/\text{H}] = -1.50$, $[\alpha/\text{Fe}] = +0.3$, and an age of 10 Gyrs has $\log g = +0.50$ and $M_V = -2.40$. Figures 8-10 indicate that whether one considers M_V , $\log g$, or T_{eff} as the independent variable, metallicity differences do not seem to have significant effects on the derived macroturbulence relations.

7. REVISED ROTATIONAL VELOCITIES FOR THE FULL CFA SAMPLE

7.1. Red Horizontal Branch Stars

7.1.1. Macroturbulence

Equation 1 offers us an opportunity to estimate stellar rotational velocities for the stars observed at CfA but not at CFHT, if we have some knowledge of ζ_{RT} . In the case of the RHB stars, this turns out to be a vexing problem.

C2007 observed that macroturbulence might explain the monotonic rise in line broadening with increasing effective temperature seen in their sample of 20 field RHB stars. The suggestion relied primarily on the finding by Gray & Toner (1986) that ζ_{RT} is a significant function of spectral type (i. e., temperature) within individual luminosity classes. Figure 11 shows a modified version of Figure 12 from C2007. Filled circles represent the line broadenings reported by C2003 and C2007, with the red ones representing stars for which we have derived rotational and macroturbulent velocities (Table 2). Open squares depict $V_{\text{rot}} \sin i$, and open triangles show ζ_{RT} . If we focus on the stars in red (from Table 2), we note the near-constancy of the macroturbulent dispersion, ζ_{RT} , from $T_{\text{eff}} \approx 5300$ K to 6200 K. The value appears to be constant, unlike that predicted by Gray & Toner (1986), although the temperature spread is not large, and the sample size is small.

There is a more fundamental concern. The mean value of ζ_{RT} for the seven RHB stars observed at CFHT is $9.1 \pm 0.7 \text{ km s}^{-1}$. If Equation 1 is correct, then none of the other thirteen RHB stars observed only at CfA should have V_{broad} values smaller than that, but Table 4 contains several values near 4 km s^{-1} . Figure 11 shows that the seven stars observed at CFHT are a bit hotter than the thirteen stars observed only at CfA. If ζ_{RT} depends on T_{eff} , as expected, could that explain the disagreement? We answer that question by considering only the stars in the narrow temperature range of 5200 K to 5600 K. The three stars observed at CFHT have $\langle \zeta_{\text{RT}} \rangle = 9.7 \pm 1.1 \text{ km s}^{-1}$ ($\sigma = 2.0 \text{ km s}^{-1}$). The twelve stars observed only at CfA have $\langle V_{\text{broad}} \rangle = 6.1 \pm 0.5 \text{ km s}^{-1}$, significantly lower than Equation 1 would predict.

Are the CfA results reliable at such low V_{broad} values? Recall that the CfA instrumental resolution is about 8.5 km s^{-1} . Six of the twenty RHB stars studied by C2003 and C2007 were also studied by Behr (2003), using higher resolution and higher-S/N spectra, and the mean difference in derived line broadenings for those six stars is only $+0.8 \pm 0.4 \text{ km s}^{-1}$, $\sigma = 1.0 \text{ km s}^{-1}$. For the two stars common to both sets of studies and with the lowest line broadening, Behr (2003) reports values of 6.6 and 5.4 km s^{-1} for BD+11 2998 and BD+9 3223, while C2003 found 6.8 and 4.8 km s^{-1} , respectively. The CfA V_{broad} values

appear to be reliable.

The observational bias of our program may be partly to blame. Most of the stars we observed were selected for study because of their larger-than-average V_{broad} values. If that also means that we have selected stars with larger-than-average ζ_{RT} values, then we might understand the discrepancy between the CFHT results for ζ_{RT} compared to the smaller values of V_{broad} for the remaining RHB stars. But if that is the explanation, then the validity of Equation 1 must be questioned because in that case because ζ_{RT} would itself be highly variable even within a narrow range of temperature.

In the absence of a simple explanation, we're forced to conclude that whereas the macroturbulence of red giants appears well-behaved (see Figures 8 to 10), that is not the case for RHB stars. This might be due to short-term variability of the phenomenon, for example. It might also be due to differences in evolutionary state that we cannot readily discern in field stars. For example, some of the field stars may have begun core helium burning with a surface temperature cooler than the instability strip; what we would call zero-age red horizontal branch stars. Other stars may have begun core helium burning within the instability strip (as RR Lyrae variables) or even hotter (BHB stars). There is a trend among globular clusters' horizontal branches such that the more metal-poor clusters tend to have horizontal branches populated mostly by BHB stars while the more metal-rich clusters favor RHB stars. Most BHB stars eventually evolve back across the H-R diagram en route to the asymptotic giant branch, so more highly evolved stars now in the RHB domain might be distinguishable statistically by lower metallicities. Let us consider the thirteen stars observed at CfA for which we do not have CFHT spectra. The seven stars with $V_{\text{broad}} \leq 6 \text{ km s}^{-1}$ have $\langle[\text{Fe}/\text{H}]\rangle = -1.99 \pm 0.23$ ($\sigma = 0.62$), while the six other stars, with $6.8 \leq V_{\text{broad}} \leq 9.7 \text{ km s}^{-1}$, have $\langle[\text{Fe}/\text{H}]\rangle = -1.61 \pm 0.19$ ($\sigma = 0.47$). There is marginal evidence for the stars with smaller broadening values being more metal-poor (and more likely to have evolved away from the BHB and now be more luminous and slightly larger in radius than zero-age RHB stars). The argument fails, however, when we consider the seven RHB stars in Table 2 with large rotational velocities and large ζ_{RT} , since $\langle[\text{Fe}/\text{H}]\rangle = -2.02 \pm 0.15$ ($\sigma = 0.39$).

We believe that the simplest interpretation at this point is to admit that the RHB stars do not share a well-defined relationship between macroturbulent dispersion and effective temperature.

7.1.2. Rotational Velocities

While we are not confident in our ability to “remove” the contribution of macroturbulence to the values of $V_{\text{broad,CfA}}$ using Equation 1, we may still estimate rotational velocities for the other thirteen RHB stars using Equation 2. The basic stellar parameters for these stars, taken from C2003 and C2007, are given in Table 4, which includes the results from the application of Equation 2. Figure 12 shows the results, with filled circles representing $V_{\text{rot}} \sin i$ values from Table 2 and open circles representing values deriving employing Equation 2. As expected, the stars observed at CFHT have larger rotational velocities, due to our bias toward stars with larger line broadening. Excluding the anomalous star HD 195636, the average rotational velocity for the remaining nineteen RHB stars is $3.3 \pm 0.8 \text{ km s}^{-1}$ ($\sigma = 0.8 \text{ km s}^{-1}$).

There is an apparent trend in the upper limits of $V_{\text{rot}} \sin i$ as a function of T_{eff} , with lower values at cooler temperatures (again, we neglect HD 195636). We do expect some sort of trend, if all six stars have identical amounts of rotational angular momentum and have comparable values of rotational axis inclinations. In that particular case, since $L \propto R^2 T_{\text{eff}}^4$ and the rotational angular momentum $J \propto MR^2$, then for equal masses, $V_{\text{rot}} \sin i \propto T_{\text{eff}}^2$. Using a log-log calculation we found that the six RHB stars with $V_{\text{rot}} \sin i$ values in Table 2 define $V_{\text{rot}} \sin i \propto T_{\text{eff}}^{5.6}$, which is shown as the dashed line in Figure 12. However, a straight line, $V_{\text{rot}} \sin i \propto T_{\text{eff}}$, provides almost as good a representation of the limited data, so no definitive conclusions may be drawn.

7.1.3. Comparison of Rotation in Blue and Red Horizontal Branch Stars

Finally, we can infer one interesting result, somewhat related to the issue raised above regarding rotational angular momentum as a function of temperature. Kinman et al. (2000) provided estimates of $V_{\text{rot}} \sin i$ for 30 blue horizontal branch (BHB) stars. The question we ask is whether the RHB stars we have studied show as large a range in rotational velocities as BHB stars, when allowance is made for the different stellar radii and moments of inertia. Because the method employed by Kinman et al. (2000) was based on the full width at half maximum of the $\lambda 4481 \text{ Mg II}$ line, and their spectral resolving power was only about 15 km s^{-1} , we ask what fractions of their BHB sample were found to have $V_{\text{rot}} \sin i$ larger than 15 and 20 km s^{-1} , and then ask what fractions of our RHB have similar rotational velocities when allowances are made for the different stellar radii.

We consider first the BHB sample. We derived stellar radii by converting the $\log g$ values into radii, assuming a stellar mass of $0.7 M_{\odot}$. This is a somewhat smaller value

than the mass we adopted for the RHB stars, $0.8 M_{\odot}$, and leads to a mean stellar radius of $3.3 R_{\odot}$ (excluding BD+32 2188 because the radius derived from its $\log g$ value, $11.8 R_{\odot}$, suggests it is not a BHB star). Six of the remaining 29 BHB stars (21%) have estimated $V_{\text{rot}} \sin i \geq 20 \text{ km s}^{-1}$, and 10 of them (34%) have $V_{\text{rot}} \sin i \geq 15 \text{ km s}^{-1}$. To compare to the RHB sample of Table 2, we must reduce the $V_{\text{rot}} \sin i$ limits by the ratio of the stellar radii, $(3.3/7.5)$, so the 20 km s^{-1} limit becomes 8.8 km s^{-1} and the 15 km s^{-1} limit becomes 6.6 km s^{-1} . Any difference in mass between the more massive RHB stars and the lower mass BHB stars would lower these limits further. Of the 7 RHB stars in Table 2, three (43%) have $V_{\text{rot}} \sin i \geq 8.8 \text{ km s}^{-1}$, and five (71%) have $V_{\text{rot}} \sin i \geq 6.6 \text{ km s}^{-1}$. This small sample would suggest that the RHB stars show a higher fraction of relatively rapid rotators than do the BHB stars, but we reiterate that the stars listed in Table 2 were selected on the basis of large V_{broad} values, so we must, in fact, include the thirteen other RHB stars, for which we have only estimated $V_{\text{rot}} \sin i$. The mean radius of the 20 RHB stars is $8.0 R_{\odot}$, so the 20 and 15 km s^{-1} limits for BHB stars are now 8.3 and 6.2 km s^{-1} , respectively, again neglecting mass differences. None of the thirteen RHB stars have $V_{\text{rot}} \sin i$ values larger than 4 km s^{-1} , so the percentage of RHB stars with $V_{\text{rot}} \sin i$ greater than 8.3 and 6.2 km s^{-1} drops to 15% and 25%, compared to the BHB stars' values (scaled for radius) of 21% and 34%.

RHB stars may show another similarity to BHB stars in the distribution of their rotational velocities. Peterson, Rood, & Crocker (1995) found a bimodal distribution of rotational velocities in the metal-poor globular cluster M13, which has a predominantly blue horizontal branch. Behr (2003) noted an apparent bimodal distribution in the rotational velocities of metal-poor field BHB stars as well. Based only on one star, HD 195636, there might also be a “bimodality” in the rotational velocity distribution of RHB stars.

Unfortunately, the small sample sizes prohibit any firm conclusions, except that there is no compelling evidence that the rotational angular momentum of RHB stars is any smaller than that of BHB stars.

7.2. Rotation of Red Giant Branch Stars

7.2.1. CFHT Data

Figure 13 shows the rotational velocities derived from the Fourier transform analyses as a function of visual absolute magnitude for the stars in Tables 2 and 3, including giants, bright giants, and supergiants.

Consider the spread in $V_{\text{rot}} \sin i$ values for the disk giants. (As before, we exclude

β Sge and λ Peg.) Sixteen of the eighteen disk giants have $V_{\text{rot}} \sin i$ values between 1.5 and 3.5 km s⁻¹, a quite narrow range. The halo giants appear to be more evenly spread out in $V_{\text{rot}} \sin i$, from about 0 to 5.5 km s⁻¹. Both distributions are puzzling. For example, if we assume that all the halo RGB stars have similar rotational velocities, the distribution in $V_{\text{rot}} \sin i$ is not consistent with the expected distribution of viewing angles. If $V_{\text{rot}} = 5.0$ km s⁻¹, we expect to find almost two thirds of the stars with $V_{\text{rot}} \sin i \geq 3.0$ km s⁻¹, but only about one sixth of the stars would have $V_{\text{rot}} \sin i \leq 2.0$ km s⁻¹. Instead we find five out of the twelve (42%) with the higher rotational velocities, and half with the lower velocities. While the statistics are weakened by the small sample size, it appears that more is at work here than just geometry.

7.2.2. CfA Data

Equations 1 and 2 allow us, in principle, to estimate $V_{\text{rot}} \sin i$ for all of the 116 red giants in the CfA program (C2003, C2007). In the case of Equation 1, we must adopt some representation of ζ_{RT} , but Equations 4 through 6 appear to be well-behaved.

For several reasons, we prefer to explore the behavior of the rotation of this larger sample of metal-poor field red giants in a slightly different fashion. As noted already, projection effects compromise the results for individual stars. Figure 8 shows that the relation between ζ_{RT} and M_V appears well-behaved, but there is scatter among the individual stars, so the correction is best treated in a statistical fashion. Finally, while Figure 9 of C2007 shows that the V_{broad} values determined by C2003 and C2007 are good measures of line broadening down to values as low as 3 km s⁻¹ (despite an instrumental resolution of 8.5 km s⁻¹), uncertainty remains for each individual star. We conclude that it is best to approach the behavior of rotational velocities derived in the above fashion in a statistical manner.

We began our analysis by removing three stars from the CfA sample, all of them binaries with short periods and, hence relatively close separations, where tidal effects of a companion may induce or inhibit the rotation of the primary star. All three stars have unusually small orbital eccentricities, consistent with tidal interactions. With BD+30 2034, BD+18 2890, and CD-37 14010 removed from the sample, we sorted the remaining 113 metal-poor red giants by M_V and averaged the results within six bins, chosen simply so that the five more luminous bins have equal numbers of stars (20), while the lowest luminosity bin has 13. Table 5 contains the results, including $\langle M_V \rangle$, $\langle R/R_{\odot} \rangle$, and $\langle V_{\text{broad}} \rangle$. The Table also includes the error, σ , and the error of the mean, σ_{μ} , for each quantity. The last two columns of Table 5 include the resultant mean rotational velocity, obtained

using $\langle V_{\text{broad}} \rangle$ and Equations 4 and 1, and Equation 2, respectively. In cases where the macroturbulence value exceeded V_{broad} , we set $V_{\text{rot}} \sin i$ to zero. Note that the results for the most luminous stars obtained using Equation 2 agree well with the mean results for the twelve stars observed at CFHT ($\langle M_V \rangle = -2.0$; $\langle V_{\text{rot}} \sin i \rangle = 2.3 \text{ km s}^{-1}$).

Figures 14 and 15 show the results. In the former case we have employed Equations 1 and 4, while in the second case we used Equation 2. We have plotted the mean rotational velocities as a function of stellar radius, which we assume, to first order, tracks the rotational angular momentum since all the stars should have very similar masses and mass distributions. The two binned samples show zero or near-zero rotation at all radii (and luminosities) except for the largest radii. This contradicts any stellar evolution that includes conservation of angular momentum, so either the surface has acquired extra rotation from internal sources or from external ones (such as absorption of a large planet), or the line broadening to which we refer as rotation is something else.

7.2.3. Discussion

The results of Figures 14 and 15 are hard to understand. C2003 and C2007 discussed the concept of transport of internal angular momentum to the surface layers, but that should appear at the radius and luminosity when the convection zone reaches its deepest penetration. Conceivably, Figure 15 is showing such an effect at $M_V \approx -0.7$. But that still does not explain the rotation seen (only) among the largest radii, most luminous stars. The planet search effort of Sozzetti et al. (2006) suggests that absorption of planets is not sufficiently common to explain the results, either. The appearance of additional (admittedly small) line broadening among only the most luminous metal-poor red giants invites a comparison with two other phenomena that likewise appear favored among such stars: velocity jitter and mass loss.

C2003 and C2007 summarized the appearance of jitter in metal-poor red giants. Jitter becomes increasingly common, with typical velocity variations of about 2 km s^{-1} for $M_V < -1.4$. For the stars studied as part of this program, a careful consideration of the results in Tables 2 and 3 shows that all five of the stars with $V_{\text{rot}} \sin i \geq 3.0 \text{ km s}^{-1}$ show velocity jitter, defined in C2003 and C2007 as stars with $P(\chi^2) \leq 10^{-6}$. Of the 12 red giants in Tables 2 and 3, the mean rotational velocity for the 8 stars showing velocity jitter is $2.9 \pm 0.7 \text{ km s}^{-1}$, compared to $1.1 \pm 0.5 \text{ km s}^{-1}$ for the other 4 stars without detectable velocity jitter.

In Figure 16 we display the results for individual stars that went into the bins of Table 5

and Figure 15. Stars displaying velocity jitter are shown as filled circles. The highest luminosity bin in Figure 15 contains the twenty metal-poor red giants with $M_V \leq -1.5$. Inspection of Figure 16 shows that 11 of the 17 stars in that bin with $V_{\text{rot}} \sin i \geq 3.0 \text{ km s}^{-1}$ show jitter. Clearly velocity jitter is related in some way to the excess line broadening. Does more rapid rotation among the most luminous stars induce jitter? Does velocity jitter masquerade as rotational broadening in some fashion? Or are both phenomena, excess line broadening and velocity jitter, symptoms of the same cause?

Mass loss may be another key to the puzzle. Smith et al. (1992), Dupree & Smith (1995), and Cacciari et al. (2004) studied Ca II K₂ line profiles in metal-poor giants, finding that for $M_V < -1.7$, the line emission is weaker on the violet side than on the red side, so that the ratio of violet to red emission line flux, V/R, is less than unity for the most metal-poor stars. That ratio indicates mass outflow, and it is therefore interesting that we have three phenomena, excess line broadening, velocity jitter, and mass outflow, that appear only at the high luminosities found near the red giant branch tip for metal-poor stars. Surely Occam's Razor suggests a common cause.

Recently, Dupree et al. (2007) discussed the mass outflow on the basis of $\lambda 2800$ Mg II absorption profiles in metal-poor stars, finding that the V/R asymmetry indicative of mass loss appears at somewhat fainter luminosities than for the Ca II K₂ asymmetry, or that of H α . In Figure 17 we show how Ca II and Mg II V/R ratios vary among stars observed by C2003, C2007, and in this paper. As in the case of jitter, it is clear that high luminosity favors both excess line broadening as well as mass loss. Further, as Dupree et al. (2007) stressed, the V/R ratios in some stars are variable, suggesting that mass loss is episodic. Thus some of the stars in Figure 17 with V>R may be temporarily stable in terms of mass loss.

Dupree et al. (2007) also noted that the mass loss decreases at lower metallicities, although the trend is weak. Mass loss remains significant in halo giants, despite the lower metallicities and especially the greater ages of halo giants compared to disk giants. This is unexpected for mass loss driven by magnetic processes, but might be explicable in terms of acoustic shock wave heating of the chromospheres of metal-poor giants (Cuntz et al. 1994). The models employed in that paper suggested velocity variations of a few km s^{-1} with periods probably shorter than pulsation, so this might be a mechanism for producing velocity jitter as well as additional line broadening.

Another explanation is that pulsation may drive heating and mass loss (Smith & Dupree 1988). Pulsation is an attractive model since it could also explain velocity jitter and possibly extra line broadening due to the accelerations present in a pulsating atmosphere. C2003 drew attention to the apparent periodicity in the velocity jitter of HD 3008 (172

days; amplitude 1.55 km s^{-1}) and BD+22 2411 (186 days; amplitude 0.96 km s^{-1}). The periods are long compared to known long-period variables in metal-poor clusters, but the periodicity is certainly suggestive. It would be worthwhile to explore more carefully the line broadening, radial velocity, and mass loss together in metal-poor luminous giants on a variety of timescales.

8. CONCLUSIONS

We have obtained high-resolution, high-S/N spectra for 12 metal-poor field RGB stars and 7 metal-poor field RHB stars. Fourier transform analyses have yielded good estimates for the macroturbulence dispersion, ζ_{RT} , and the rotation velocity, $V_{\text{rot}} \sin i$, for all the stars. We obtained consistent results for HD 29574, which was observed during both observing runs, and for η Ser, which had been studied previously by Gray & Pallavicini (1989). It is good to recall that we selected our stars from the C2003 and C2007 samples of 116 RGB stars and 20 RHB stars, and with a bias toward stars with larger line broadening values (referred to as rotational velocities by C2003). The RGB stars appear to show very similar macroturbulence behavior as a function of luminosity, gravity, and temperature as do disk giants. The twelve RGB stars studied here, however, show a larger range in rotational velocities, with half showing values of 2.0 km s^{-1} or less, and five having values in excess of 3.0 km s^{-1} . For the seven field RHB stars, we confirm the rapid rotation of HD 195636 discovered by Preston (1997). When allowance is made for the star's larger radius compared to BHB stars, its rotational angular momentum is comparable to the largest seen in field BHB stars.

We have explored the use of two empirical methods, neither justified physically, to attempt to exploit the more extensive data on line broadening from C2003 and C2007. The derived rotational velocities of the 13 field RHB stars are, as expected from the CfA results, modest. To compare our results with the much lower resolution BHB data from Kinman et al. (2000), we consider the percentages of BHB stars whose rotation rates are comparable to the spectral resolution, and then make allowances for the differences in radii between the BHB stars and our sample of RHB stars. We find that the RHB stars have fewer rapidly rotating stars than does the BHB sample studied by Kinman et al. (2000).

Both algorithms were applied to binned samples of the field RGB stars, so that statistical fluctuations would be diminished. All but the bin containing the most luminous stars ($M_V \leq -1.5$) showed nearly zero mean rotation, as expected for the large radii. It is clear that the most luminous metal-poor field RGB stars show enhanced rotation or some other source of line broadening, as found initially by C2003. Unlike the results from C2003,

however, the line broadening is relatively modest, on average being 2 km s^{-1} or 4 km s^{-1} , depending on which algorithm is employed. Our CFHT observations did not extend to the lower luminosities, but are consistent with this result. The twelve RGB stars studied had $\langle M_{\text{rot}} \rangle = -2.0$ and $\langle V_{\text{rot}} \sin i \rangle = 2.3 \text{ km s}^{-1}$.

We draw attention to the fact that the transition in luminosity between negligible and significant rotation occurs at about the same M_V value as the appearance of velocity jitter and mass loss. This is highly suggestive of a common underlying physical origin, which may be a sign of shock waves and acoustic heating of chromospheres (Cuntz et al. 1994) or pulsation (Smith & Dupree 1988). We recommend a dedicated monitoring program of a few key stars to compare timescales and the presence of line broadening, velocity variations, and mass loss.

We acknowledge financial support from the National Science Foundation to the University of North Carolina through grant AST0305431 and to Bowling Green State University through grant AST0307340.

Table 1. Observational Data

Star	λ	HJD-2,450,000	V	Exp	S/N ^a	V_{rad}	σ	Comments
HD 3008	6150	3366.7716	9.70	40	175	-81.83	0.34	RGB; CM Cet; jitter
BD-18 271	6150	4015.8939	9.85	90	145	-210.54	0.19	RGB; jitter
CD-36 1052	5430	3366.8083	10.00	70	150	+304.36	0.32	RHB
HD 23798	6150	3366.8681	8.32	25	210	+88.83	0.54	RGB
HD 25532	5430	4016.9720	8.24	80	175	-111.88	0.34	RHB
BD+6 648	6150	4015.1177	9.09	270	285	-142.41	0.31	RGB
HD 29574	6150	3366.8934	8.38	60	155	+17.86	0.37	RGB; HP Eri; jitter
	6150	4015.0694		35	250	+17.67	0.48	
HD 82590	5430	3366.9454	9.42	75	180	+214.31	0.37	RHB; NSV 4526
BD+22 2411	6150	3367.0135	9.95	90	160	+35.05	0.26	RGB; jitter
HD 106373	5430	3367.1146	8.91	75	190	+83.68	0.21	RHB
HD 110281	6150	3367.0801	9.39	45	170	+139.90	0.51	RGB; KR Vir; jitter
HD 165195	6150	4011.7779	7.34	120	380	+0.50	0.40	RGB; V2564 Oph; jitter
HD 184266	5430	4016.7436	7.57	50	250	-349.20	0.39	RHB
HD 187111	6150	4015.8079	7.75	40	395	-186.16	0.15	RGB
HD 195636	5430	4016.7877	9.57	140	130	-258.34	1.62	RHB
HD 214925	6150	4015.7595	9.30	50	215	-327.26	0.60	RGB; jitter
HD 214362	5430	4016.9199	9.10	60	105	-92.48	0.14	RHB
HD 218732	6150	4015.8478	8.47	40	270	-294.24	0.25	RGB; LS Aqr; SLSB; jitter
HD 221170	6150	4009.8693	7.71	100	260	-121.69	0.40	RGB; NSV 14589
η Ser	6150	3981.7138	3.26	20	300	+12.24	0.15	RGB; check; NSV 10675

^aS/N values are per pixel. A typical resolution element is 2.3 pixels.

Table 2. Line Broadening Results

Star	M_V	T_{eff}	$\log g$	[Fe/H]	V_{broad}	$V_{\text{rot}} \sin i$	ζ_{RT}	Comments
HD 3008	-1.5	4140	1.00	-1.43	9.2	4.4 ± 0.8	6.9 ± 0.6	RGB
BD-18 271	-2.1	4150	0.70	-1.98	7.3	0.0 ± 1.5	7.2 ± 1.0	RGB
CD-36 1052	+0.62	5890	2.50	-2.00	14.4	8.8 ± 0.8	8.9 ± 0.8	RHB
HD 23798	-1.8	4310	1.00	-1.90	5.0	0.0 ± 1.0	6.7 ± 0.6	RGB
HD 25532	+0.79	5320	2.54	-1.33	8.5	4.8 ± 1.0	7.6 ± 0.7	RHB
BD+6 648	-1.79	4160	0.87	-1.82	6.1	1.2 ± 1.5	6.6 ± 1.0	RGB
HD 29574	-2.11	3960	0.57	-2.11	10.2	3.7 ± 1.0 4.2 ± 0.7	7.4 ± 0.6 7.3 ± 0.5	RGB
HD 82590	+0.7	5960	2.70	-1.85	13.0	7.7 ± 0.6	11.0 ± 0.5	RHB
BD+22 2411	-1.7	4320	1.00	-1.95	7.3	0.0 ± 2.0	7.5 ± 0.7	RGB
HD 106373	+0.57	6160	2.70	-2.48	13.5	10.8 ± 0.7	6.5 ± 1.5	RHB
HD 110281	-2.6	3850	0.20	-1.75	11.5	5.5 ± 1.0	6.2 ± 1.0	RGB
HD 165195	-2.14	4200	0.76	-2.16	7.6	1.8 ± 0.7	6.4 ± 0.5	RGB
HD 184266	+0.7	5490	2.60	-1.87	11.7	5.0 ± 0.5	11.5 ± 0.3	RHB
HD 187111	-1.54	4260	1.04	-1.65	5.2	2.4 ± 0.5	5.5 ± 0.7	RGB
HD 195636	+0.5	5370	2.40	-2.40	21.5	22.2 ± 1.0	10.0 ± 1.5	RHB
HD 214925	-2.5	3890	0.30	-2.14	9.7	4.5 ± 0.7	8.4 ± 0.4	RGB
HD 214362	+0.6	5700	2.60	-2.20	11.1	7.5 ± 1.0	8.5 ± 0.7	RHB
HD 218732	-2.8	3900	0.20	-2.00	11.1	3.1 ± 0.5	6.4 ± 0.7	RGB
HD 221170	-1.7	4410	1.10	-1.56	7.4	1.0 ± 1.0	6.4 ± 0.5	RGB
η Ser	+1.87	4890	3.21	-0.42	4.0	1.0 ± 0.8	4.1 ± 0.5	disk RGB

Table 3. Disk Giants

Star	HR	Sp Type	[Fe/H]	T_{eff}	$\log g$	M_V	$V_{\text{rot}} \sin i$	ζ_{RT}
ξ Cyg	8079	K4.5 Ib	-0.45	4090	1.42	$-4.60^{+0.45}_{-0.37}$	1.6 ± 2.0	10.1 ± 1.0
58 Per	1454	G8 II	-0.29	4260	2.21	$-2.22^{+0.47}_{-0.38}$	6.3 ± 1.4	10.2 ± 0.9
θ Lyr	7314	K0 II	-0.01	4500	1.93	$-2.76^{+0.27}_{-0.24}$	3.6 ± 1.4	5.6 ± 0.9
θ Her	6695	K1 II	-0.24	4330	1.28	$-2.71^{+0.26}_{-0.23}$	3.4 ± 0.6	7.9 ± 0.2
λ Lyr	7192	K2.5 II	-0.02	4220	2.21	$-3.75^{+0.65}_{-0.50}$	3.2 ± 1.0	6.3 ± 0.5
π Her	6418	K3 II	-0.18	4100	1.68	$-2.10^{+0.13}_{-0.12}$	3.7 ± 0.1	4.9 ± 0.6
β Cyg	7417	K3 II	-0.17	4270	1.79	$-2.27^{+0.15}_{-0.14}$	3.0 ± 0.3	6.1 ± 0.2
γ Aql	7525	K3 II	-0.29	4210	1.63	$-3.38^{+0.24}_{-0.22}$	3.2 ± 0.5	7.0 ± 0.4
1 Lac	8498	K3 II-III	-0.12	4350	1.75	$-2.61^{+0.27}_{-0.24}$	3.6 ± 1.4	5.6 ± 0.9
α Hya	3748	K3 II-III	-0.12	4120	1.77	$-1.68^{+0.09}_{-0.09}$	0.0 ± 1.4	6.5 ± 0.9
β Sge	7488	G8 IIIa	-0.03	4850	2.79	$-1.39^{+0.22}_{-0.20}$	9.1 ± 0.7	8.2 ± 0.7
λ Peg	8667	G8 IIIa	-0.10	4800	3.20	$-1.46^{+0.19}_{-0.18}$	7.8 ± 0.4	7.8 ± 0.4
β Her	6148	G8 III	-0.27	4920	2.62	$-0.49^{+0.10}_{-0.10}$	3.4 ± 1.0	6.8 ± 1.0
η Dra	6132	G8 III	-0.21	4940	3.10	$+0.59^{+0.03}_{-0.03}$	2.2 ± 1.0	5.5 ± 1.0
α^2 Cap	7754	G8 IIIb	-0.18	5000	3.05	$+0.98^{+0.07}_{-0.06}$	3.2 ± 0.4	4.6 ± 0.3
α Cas	168	K0 III	-0.09	4610	2.71	$-1.98^{+0.09}_{-0.09}$	4.9 ± 0.4	6.2 ± 0.3
δ Tau	1373	K0 III	0.00	4940	2.85	$+0.40^{+0.10}_{-0.09}$	2.5 ± 1.0	6.2 ± 1.0
γ Tau	1346	K0 III	-0.02	4930	2.90	$+0.28^{+0.12}_{-0.12}$	2.4 ± 1.0	5.9 ± 1.0
β Cet	188	K0 III	-0.09	4820	2.87	$-0.30^{+0.05}_{-0.05}$	3.0 ± 1.0	5.9 ± 1.0
θ^1 Tau	1411	K0 III	+0.04	4960	3.17	$+0.43^{+0.09}_{-0.09}$	3.4 ± 1.0	4.9 ± 1.0
β Gem	2990	K0 III	-0.04	4850	2.75	$+1.08^{+0.02}_{-0.02}$	2.5 ± 1.0	4.2 ± 1.0
ϵ Cyg	7949	K0 III	-0.27	4730	2.89	$+0.78^{+0.03}_{-0.03}$	3.0 ± 1.0	4.2 ± 1.0
α UMa	4301	K0 III	-0.20	4660	2.46	$-1.10^{+0.04}_{-0.04}$	2.6 ± 1.0	5.2 ± 1.0
γ^1 Leo	4057	K2 III	-0.49	4470	2.35	$-0.32^{+0.07}_{-0.07}$	2.6 ± 1.0	5.2 ± 1.0
α Ari	617	K2 III	-0.25	4480	2.57	$+0.47^{+0.04}_{-0.04}$	3.1 ± 1.0	3.9 ± 1.0
β Oph	6603	K2 III	+0.02	4550	2.63	$+0.77^{+0.04}_{-0.04}$	1.6 ± 1.0	4.0 ± 1.0
α Ser	5854	K2 III	+0.03	4530	2.76	$+0.88^{+0.03}_{-0.03}$	0.0 ± 1.0	4.8 ± 1.0
α Boo	5340	K2 III	-0.60	4200	2.19	$-0.30^{+0.02}_{-0.02}$	2.4 ± 1.0	5.2 ± 1.0
η Ser	6869	K2 III	-0.42	4890	3.21	$+1.87^{+0.03}_{-0.03}$	2.0 ± 0.5	4.0 ± 0.5
ϵ Sco	6241	K2.5 III	-0.17	4560	2.49	$+0.78^{+0.04}_{-0.04}$	2.6 ± 0.5	4.3 ± 0.5
ϵ Crv	4630	K2.5 III	+0.13	4320	2.16	$-1.82^{+0.15}_{-0.14}$	2.6 ± 0.5	5.8 ± 0.5
26 Aql	7333	G8 III-IV	-0.21	4900	3.31	$+1.63^{+0.08}_{-0.08}$	2.8 ± 0.5	5.0 ± 0.5

Table 4. The Other 13 Red Horizontal Branch Stars

Star	α (J2000)	δ (J2000)	[Fe/H]	M_V	T_{eff}	$\log g$	R/R_\odot	V_{broad}	V_{rot}^a
HD 20	00:05:15.3	-27:16:18	-1.66	0.7	5350	2.5	8.2	5.9	0.8
CD-23 72	00:16:16.5	-22:34:40	-1.12	0.8	5270	2.5	8.0	8.9	3.1
HD 3179	00:34:50.6	-21:52:56	-0.92	0.9	5280	2.6	7.8	5.2	0.4
BD+44 493	02:26:49.7	+44:57:46	-2.71	0.8	5510	2.6	7.4	3.9	0.0
HD 108317 (binary)	12:24:04.4	+05:34:46	-2.48	0.5	5230	2.4	9.6	5.1	0.4
HD 110885	12:45:19.2	+01:03:20	-1.59	0.7	5330	2.5	8.2	8.2	2.5
HD 119516	13:43:26.7	+15:34:29	-2.49	0.6	5440	2.5	8.6	9.1	3.3
BD+9 2860	14:13:19.7	+08:36:40	-1.67	0.7	5240	2.5	8.6	3.9	0.0
BD+11 2998	16:30:16.7	+10:59:51	-1.46	0.8	5360	2.5	8.0	6.8	1.4
BD+9 3223	16:33:35.6	+09:06:17	-2.41	0.6	5310	2.4	8.9	4.8	0.2
BD+17 3248	17:28:14.4	+17:30:35	-2.07	0.65	5240	2.44	9.0	4.3	0.0
BD+25 3410	18:02:03.2	+25:00:41	-1.37	0.79	5740	2.69	6.7	9.7	3.9
BD-3 5215	21:28:01.3	-03:07:40	-1.64	0.7	5420	2.6	7.9	7.3	1.8

^aThese values are derived using Equation 2.

Table 5. CfA Data Binned by M_V

$\langle M_V \rangle$	N	σ	σ_μ	$\langle R \rangle$ (R_\odot)	σ	σ_μ	$\langle V_{\text{broad}} \rangle$	σ	σ_μ	$\langle V_{\text{rot}} \sin i \rangle$	
										Eq. 1	Eq. 2
-2.01	20	0.52	0.12	64.3	21.7	4.8	7.7	2.3	0.5	4.4	2.1
-1.28	20	0.37	0.08	34.9	5.8	1.3	5.2	1.7	0.4	0.0	0.4
-0.67	20	0.38	0.09	22.2	3.4	0.8	5.5	1.7	0.4	0.0	0.6
+0.07	20	0.32	0.07	14.7	2.3	0.5	4.2	1.4	0.3	0.0	0.0
+0.83	20	0.50	0.11	9.4	1.0	0.2	3.8	2.2	0.5	0.0	0.0
+1.89	13	0.68	0.19	5.4	1.0	0.3	2.9	2.5	0.7	0.0	0.0

Table 6. Comparison of Derived Rotational Velocities with Mg II and Ca II Emission line Asymmetries

Star	M_V	V_{rad}	$V_{\text{rot}} \sin i$	$V_{\text{broad}}(\text{CfA})$	$V_{\text{rot}}(\text{Eq.1})$	$V_{\text{rot}}(\text{Eq.2})$	Mg II	Ca II
HD 2796	-0.81	-61.0	...	7.0	4.1	1.6	...	V>R
HD 6755 ^a	1.50	-319.2	...	3.3	0.0	0.0	V>R	V>R
HD 6833	-0.40	-245.0	...	7.4	5.0	1.9	V<R	V=R
HD 8724	-1.11	-113.2	...	6.0	1.4	0.9	...	V>R
HD 21022	-1.17	122.3	...	5.0	0.0	0.3	...	V>R
HD 23798	-1.80	89.4	0.0	5.0	0.0	0.3	...	V=R
HD 26297 ^b	-1.48	14.8	...	0.5	0.0	0.0	...	V>R
HD 29574 ^c	-2.11	19.8	4.0	10.1	7.8	4.3	...	V<R
HD 36702	-1.90	122.7	...	6.5	1.5	1.2	...	V>R
HD 63791	0.30	-108.4	...	3.7	0.0	0.0	...	V>R
HD 83212	-0.90	109.1	...	7.3	4.5	1.8	...	V<R
HD 88609	-1.42	-38.5	...	4.0	0.0	0.0	...	V>R
HD 110281	-2.60	141.9	5.5	11.5	9.3	5.8	...	V=R
HD 118055	-1.50	-100.7	...	7.4	4.2	1.9	...	V<R
HD 122956 ^d	-0.70	166.0	...	6.3	2.9	1.1	V<R	V>R
HD 126587	-0.60	149.0	...	4.3	0.0	0.0	V>R	...
BD+1 2916	-1.76	-12.1	...	8.2	5.3	2.5	...	V>R
HD 166161	0.79	68.3	...	4.0	0.0	0.0	...	V>R
HD 175305	1.80	-181.0	...	7.1	5.8	1.7	V>R	V=R
HD 184711 ^e	-2.35	102.2	...	7.7	4.0	2.1	...	V≤R
HDE 232078	-2.15	-387.2	...	10.9	8.8	5.2	...	V=R
HD 187111 ^f	-1.54	-186.5	2.4	5.2	0.0	0.4	...	V≤R
HD 204543 ^g	-1.09	-98.4	...	5.0	0.0	0.3	...	V≥R
HD 216143	-1.4	-116.0	...	5.5	0.0	0.6	V<R	V>R
HD 218732 ^h	-2.80	-312.2	3.1	11.1	8.7	5.4	...	V<R
HD 221170	-1.70	-119.0	1.0	7.4	4.0	1.9	V<R	V>R
HD 222434 ⁱ	-1.20	8.8	...	5.0	0.0	0.3	...	V=R

^aWe employ the γ velocity for this binary system.

^bDupree & Smith 1995 cite $V_{\text{rad}} = +135 \text{ km s}^{-1}$, which we believe to be incorrect.

^cSmith et al. 1992 and Dupree & Smith 1995 both found V>R.

^dSmith et al. 1992 and Dupree & Smith 1995 both found V>R.

^eSmith et al. 1992 found V<R while Dupree & Smith 1995 found it to be uncertain. We adopt the former value.

^fSmith et al. 1992 found V<R while Dupree & Smith 1995 found V=R.

^gSmith et al. 1992 found V>R and Dupree & Smith 1995 found V≈R. Both suggested $M_V = -0.3$, but we recommend -1.09.

^hWe employ the γ velocity for this binary system.

ⁱWe employ the γ velocity for this binary system.

REFERENCES

- Baudrand, J., & Vitry, R. 2000, in Proc. SPIE, 4008, 182
- Baudrand, J., & Walker, G. A. H. 2001, PASP, 113, 851
- Behr, B. 2003, ApJS, 149, 101
- Cacciari, C., Bragaglia, A., Rossetti, E., Fusi Pecci, F., Mulas, G., Carretta, E., Gratton, R. G., Momany, Y., & Pasquini, L. 2004, A&A, 413, 343
- Carney, B. W., Latham, D. W., Stefanik, R. P., Laird, J. B., & Morse, J. A. 2003, AJ, 125, 293 (C2003)
- Cuntz, M., Rammacher, W., & Ulmschneider, P. 1994, ApJ, 432, 690
- Demarque, P., Woo, J.-H., Kim, Y.-C., & Yi, S. K. 2003, ApJS, 155, 667
- Dupree, A. K., Hartmann, L., & Smith, G. H. 1990, ApJ, 353, 623
- Dupree, A. K., & Smith, G. H. 1995, AJ, 110, 405
- Dupree, A. K., Li, T. Q. Q., & Smith, G. H. 2007, AJ, 134, 1348
- Gray, D. F. 1978, Solar Physics, 59, 193
- Gray, D. F. 1982, ApJ, 262, 282
- Gray, D. F. 1984, ApJ, 281, 719
- Gray, D. F. 1989, ApJ, 347, 1021
- Gray, D. F. 2005, The Observation and Analysis of Stellar Photospheres (New York, Cambridge University Press)
- Gray, D. F., & Pallavicini, R. 1989, PASP, 101, 685
- Gray, D. F., & Toner, C. G. 1986, ApJ, 310, 277
- Gray, D. F., & Toner, C. G. 1987, ApJ, 322, 360
- Kinman, T., Castelli, F., Cacciari, C., Bragaglia, A., Harmer, D., & Valdes, F. 2000, A&A, 364, 102
- Kurtz, M. J., & Mink, D. J. 1998, PASP, 110, 934
- Massarotti, A., Latham D. W., Stefanik, R. P., Fogel, J., Carney, B. W., & Laird, J. B. 2007, in preparation
- McWilliam, A. 1990, ApJS, 74, 1075
- Preston, G. W. 1997, AJ, 113, 1860
- Toner, C. G., & Gray, D. F. 1988, ApJ, 334, 1008

Smith, G. H., & Dupree, A. K. 1988, AJ, 95, 1547

Smith, G. H., Dupree, A. K., & Churchill, C. W. 1992, AJ, 104, 2005

Sozzetti, A., Torres, G., Latham, D. W., Carney, B. W., Stefanik, R. P., Boss, A. P., & Laird, J. B. 2006, ApJ, 649, 428

Yi, S. K., Kim, Y.-C., & Demarque, P. 2003, ApJS, 144, 259

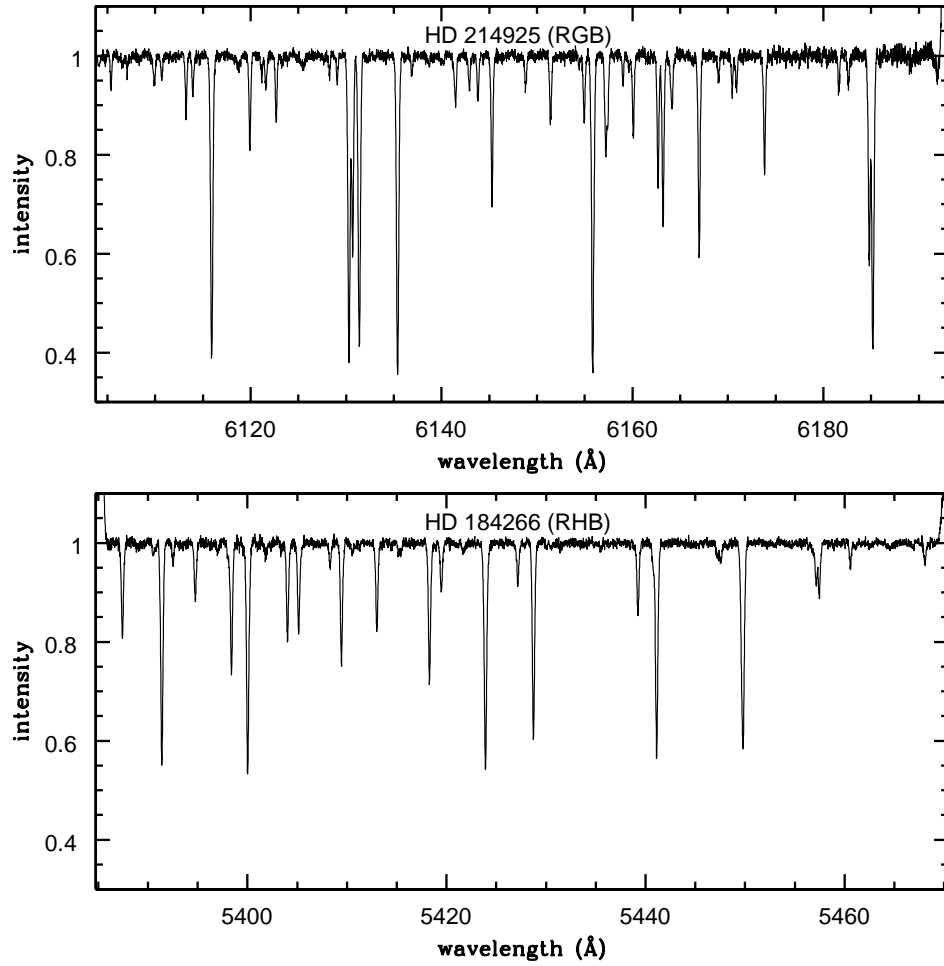


Fig. 1.— The spectral coverage for one of our twelve red giant branch stars and one of the seven red horizontal branch stars.

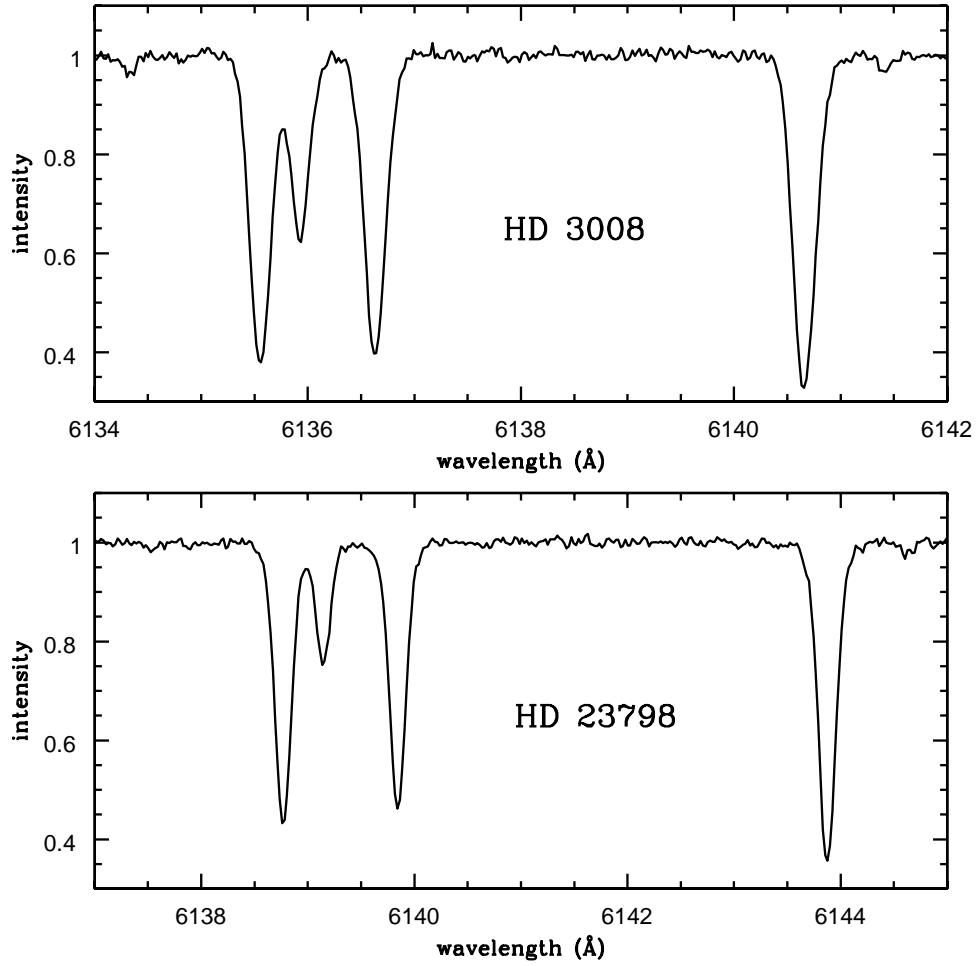


Fig. 2.— A “close-up” of the CFHT spectra of two of our program red giant branch stars. HD 3008 has slightly broader lines, as the analyses of the CfA and CFHT spectra indicated.

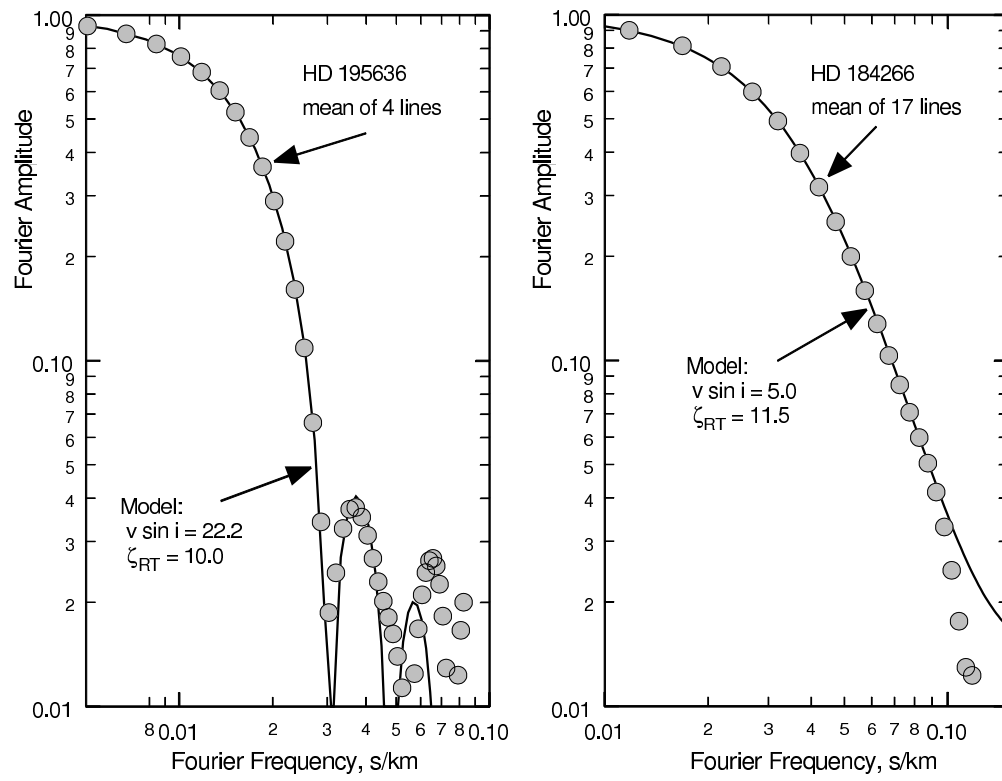


Fig. 3.— The mean residual transforms (circles) are shown with the adopted models (line) for two of our program stars.

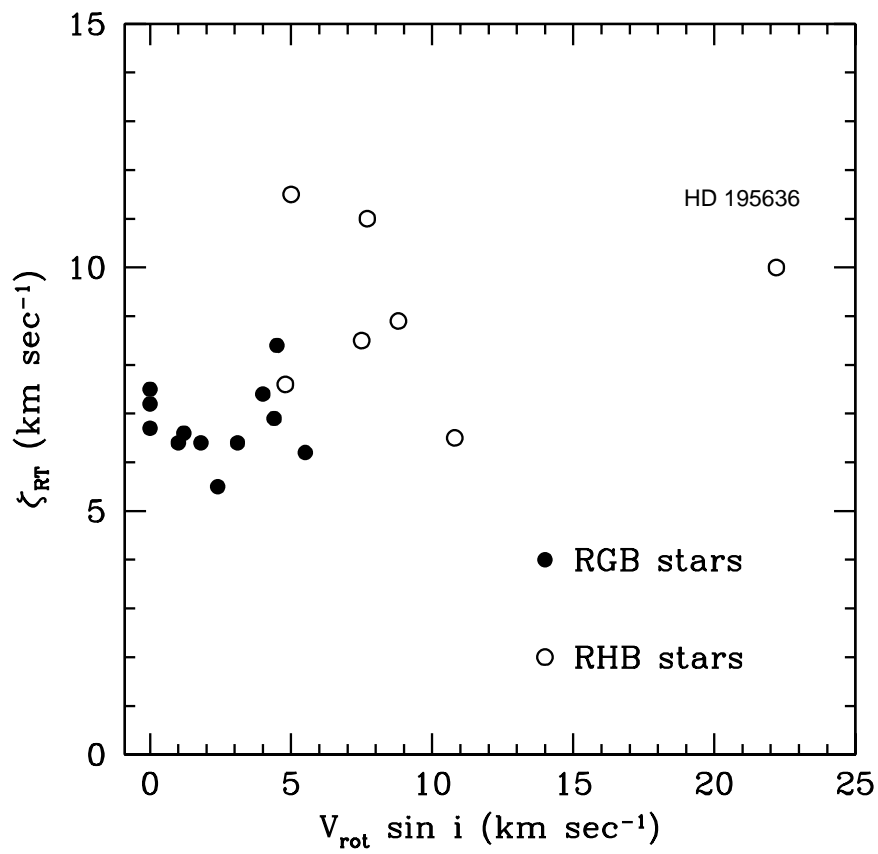


Fig. 4.— A comparison of our derived macro-turbulence dispersion values, ζ_{RT} , and rotational velocities, $V_{rot} \sin i$.

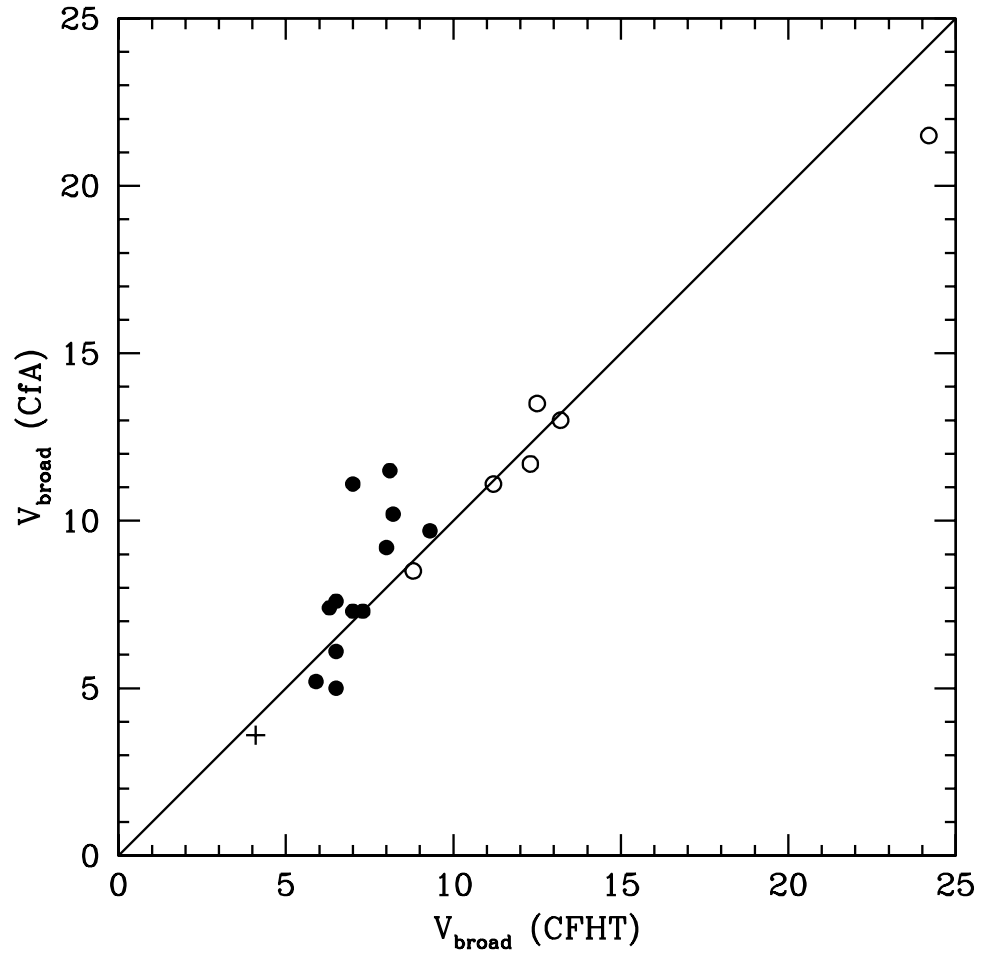


Fig. 5.— A comparison of the line broadening measured using the CfA spectra, $V_{\text{broad}} \text{ (CfA)}$ with that derived from our CFHT results using Equation 1, $V_{\text{broad}} \text{ (CFHT)}$. Filled circles are RGB stars; open circles are RHB stars; the plus sign is η Ser.

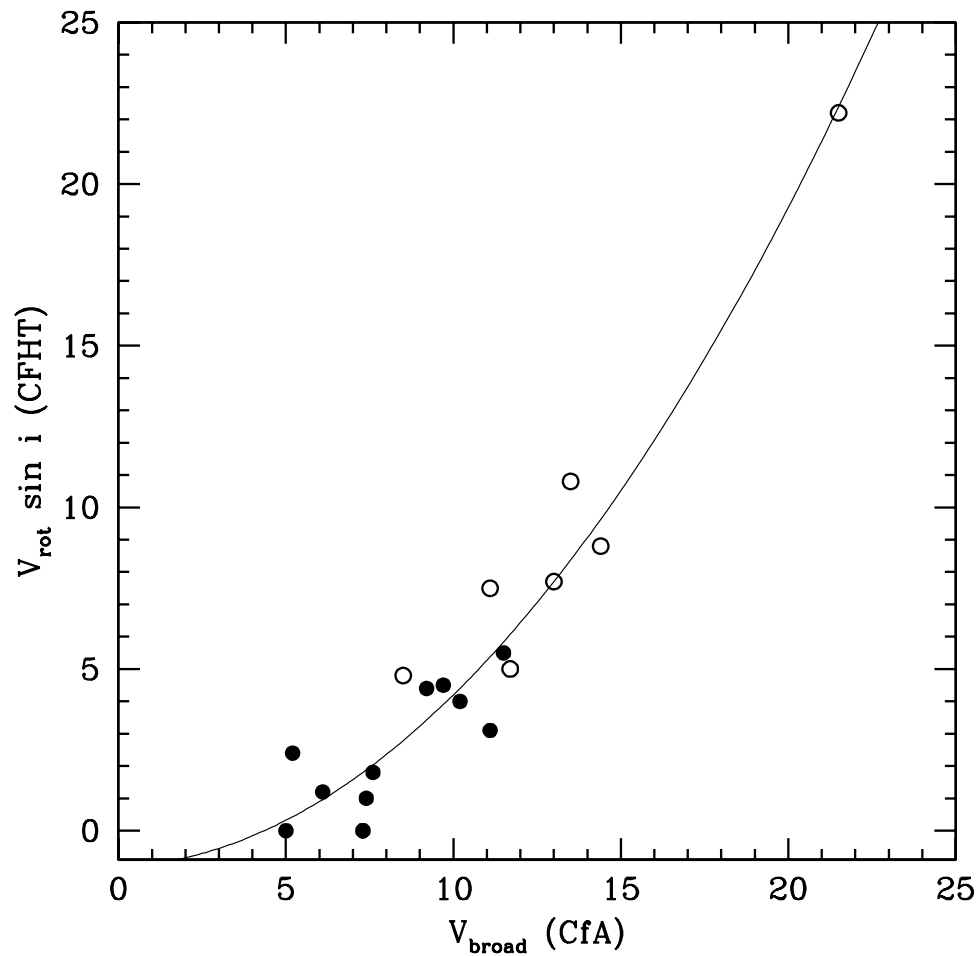


Fig. 6.— A comparison of the rotational velocity, $V_{\text{rot}} \sin i$, derived from the CfA spectra, $V_{\text{broad}} (\text{CfA})$, using Equation 2, with that measured using the CFHT spectra, $V_{\text{rot}} \sin i (\text{CFHT})$. Filled circles are RGB stars; open circles are RHB stars.

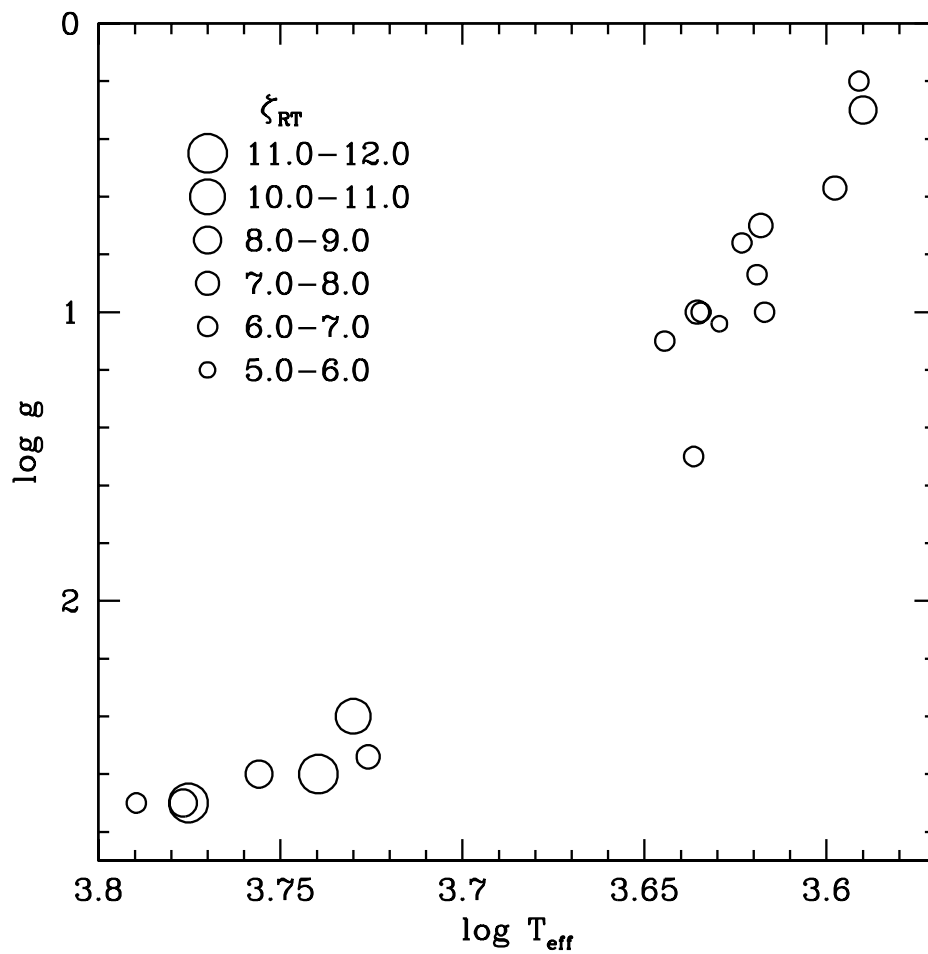


Fig. 7.— A comparison of our derived macro-turbulence dispersion values, ζ_{RT} , as a function of temperature and gravity. We employ different sizes for the data point to illustrate the different magnitudes of ζ_{RT} .

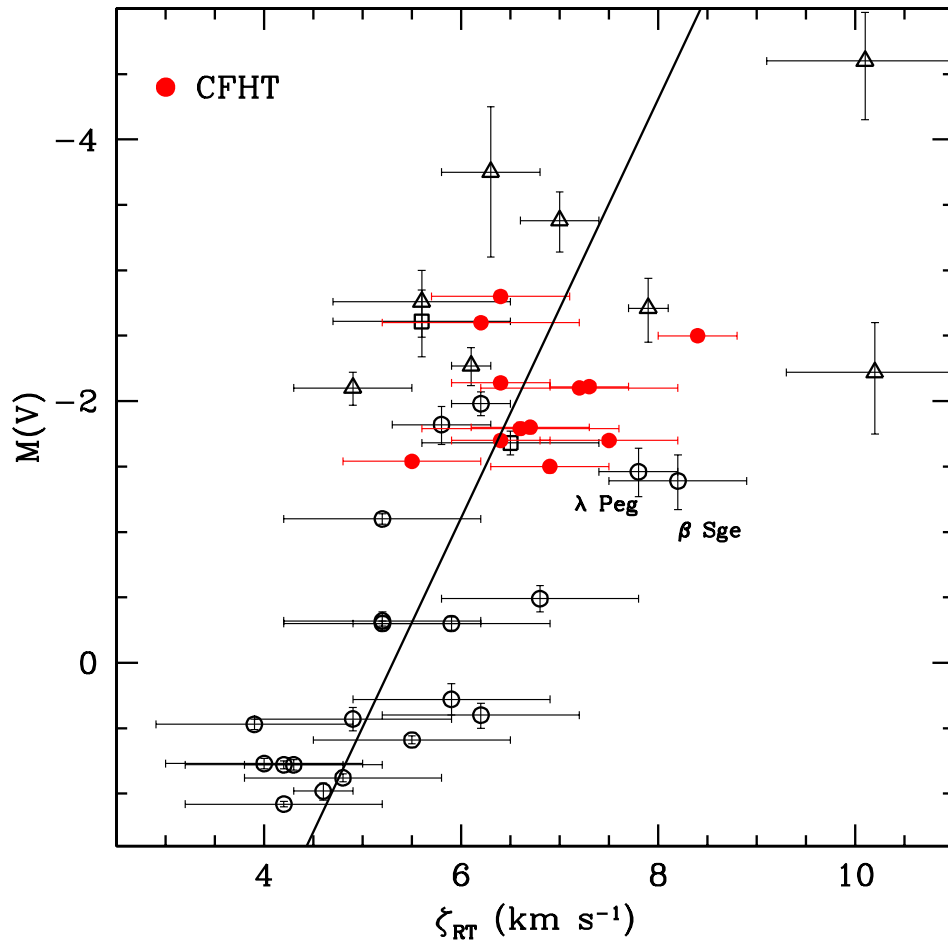


Fig. 8.— A comparison of our derived macro-turbulence dispersion values, ζ_{RT} , with M_V .

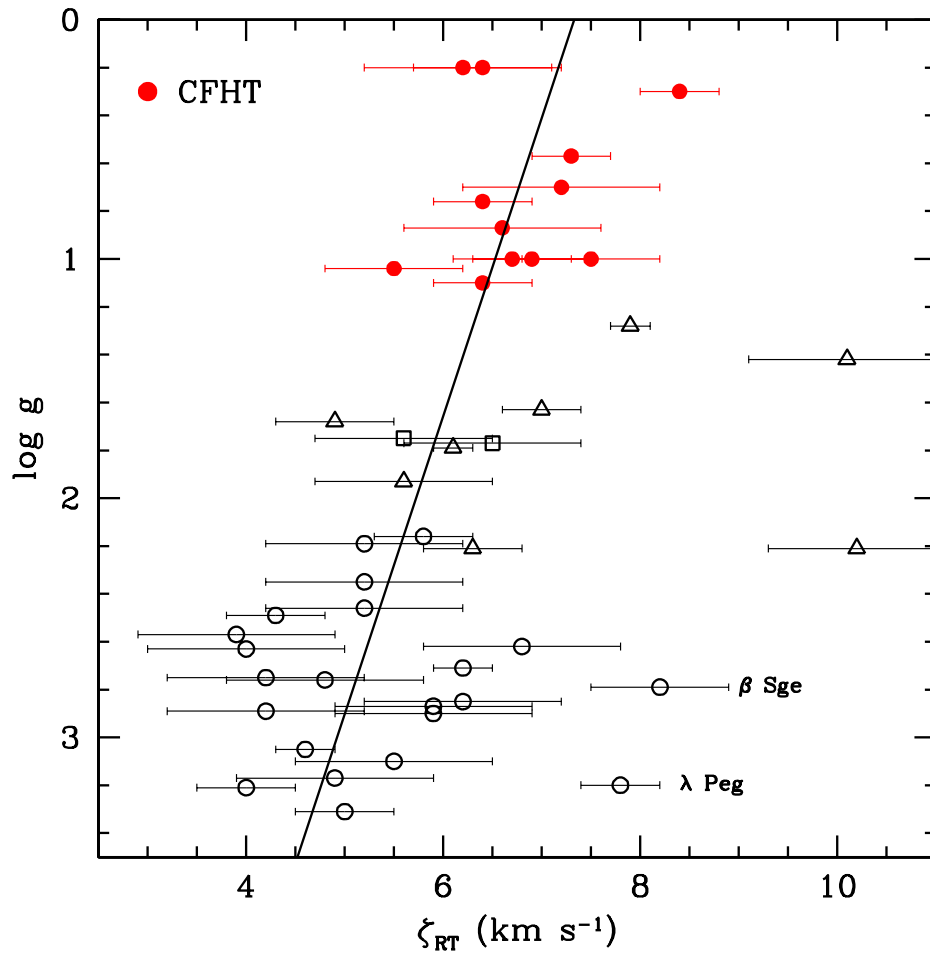


Fig. 9.— A comparison of our derived macroturbulence dispersion values, ζ_{RT} , with gravity.

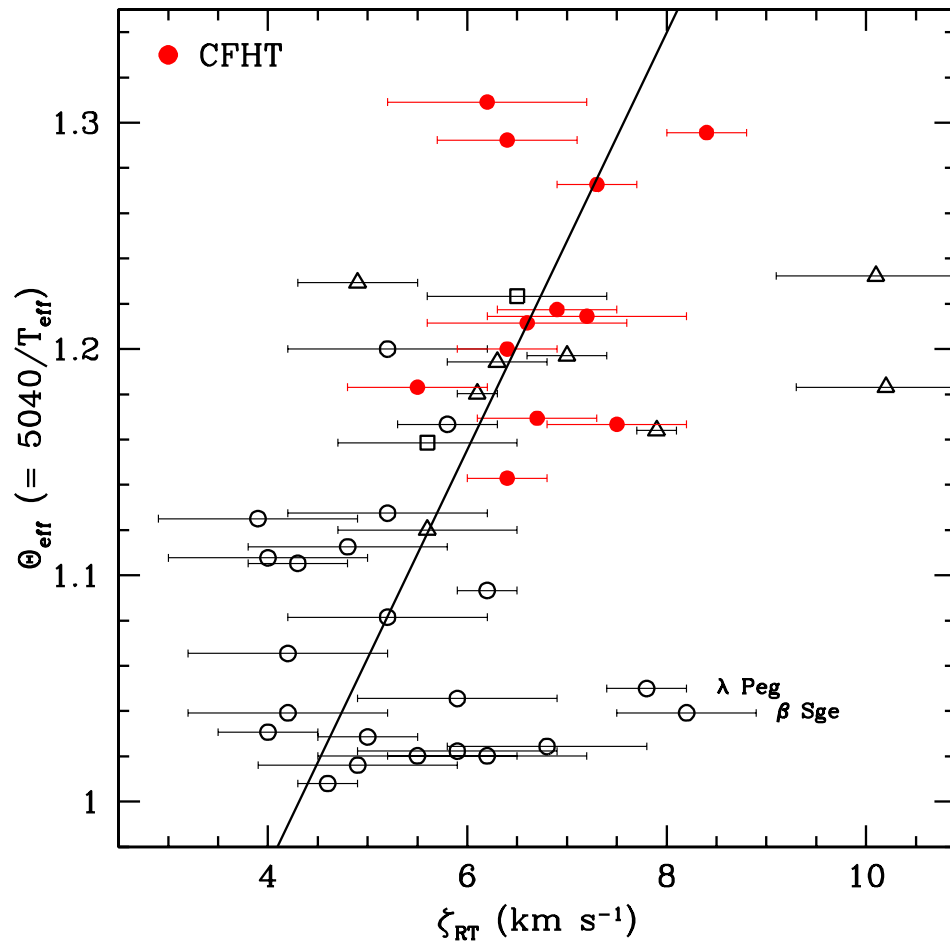


Fig. 10.— A comparison of our derived macro-turbulence dispersion values, ζ_{RT} , with Θ_{eff} ($= 5040/T_{\text{eff}}$).

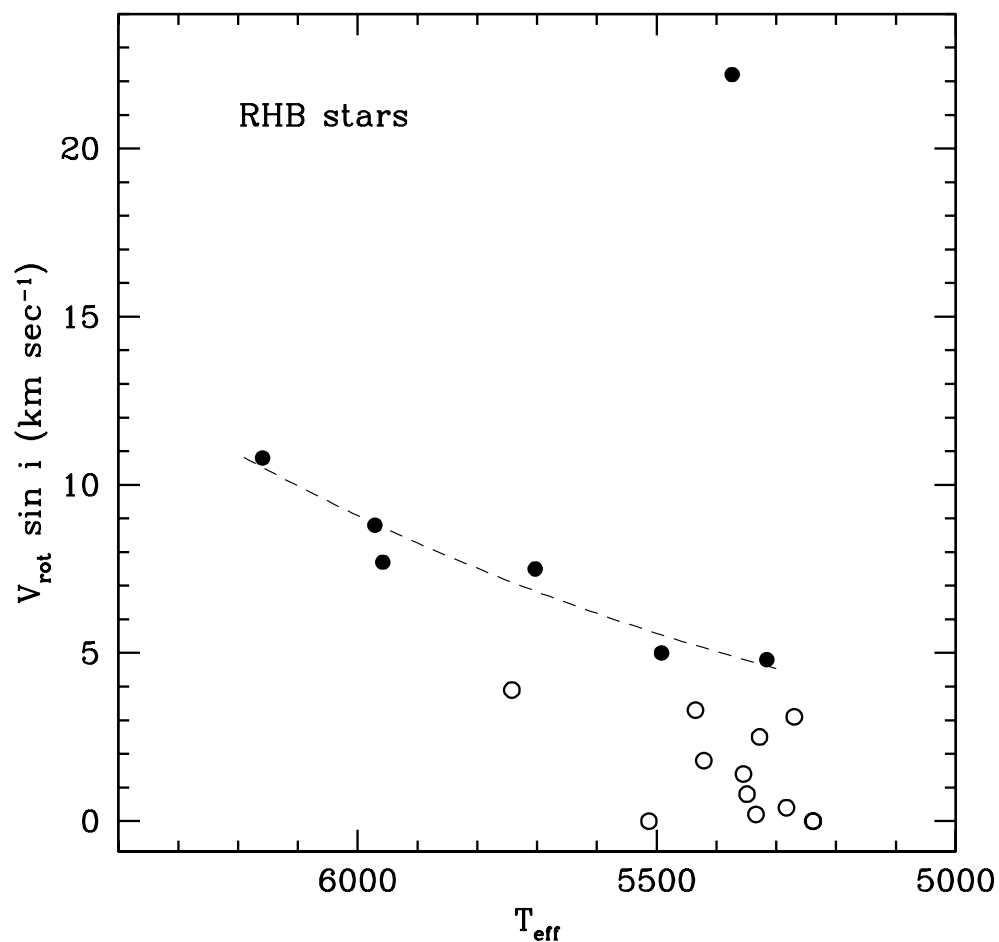


Fig. 12.— The behavior of rotational velocity, $V_{\text{rot}} \sin i$ for red horizontal branch stars as a function of T_{eff} . Filled circles are values from Table 2 while open circles depict results from Equation 2 applied to the other 13 RHB stars observed at CfA. The dashed line represents the results of a log-log relationship derived using six of the CFHT stars, $V_{\text{rot}} \sin i \propto T_{\text{eff}}^{5.6}$. We excluded HD 195636.

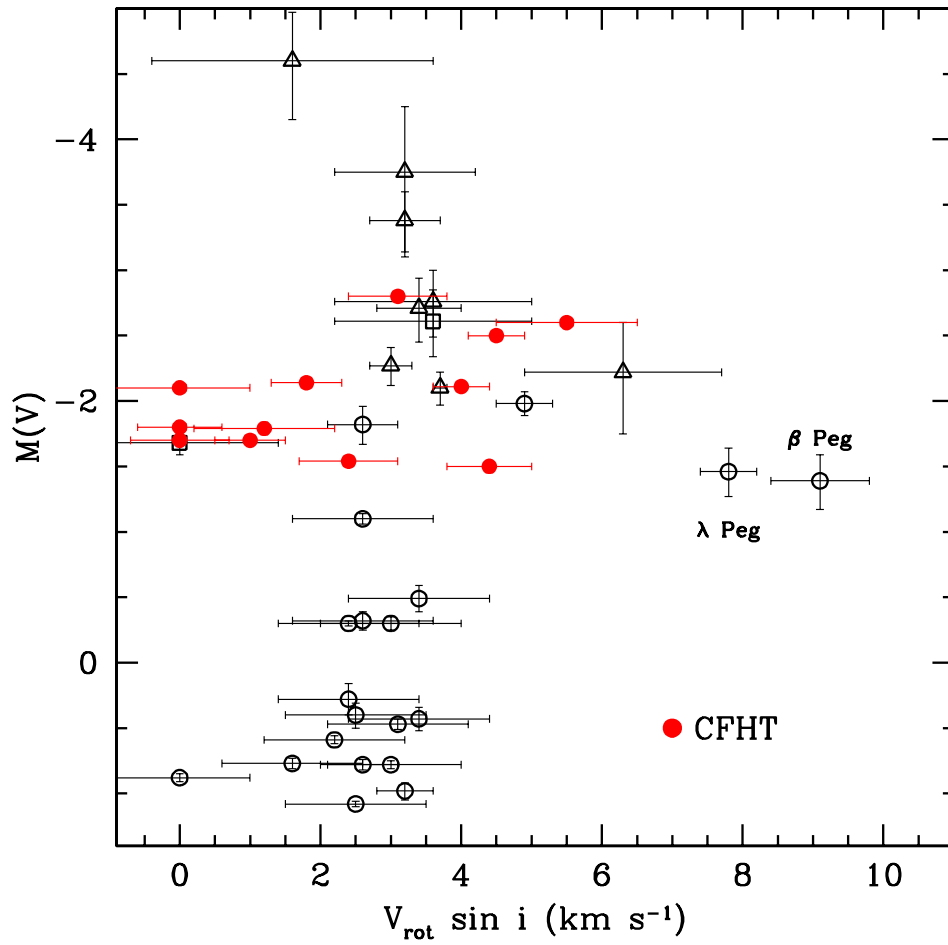


Fig. 13.— The $V_{\text{rot}} \sin i$ values for red giants derived from Fourier transform methods as a function of luminosity. Stars from Table 2 are plotted as filled red circles.

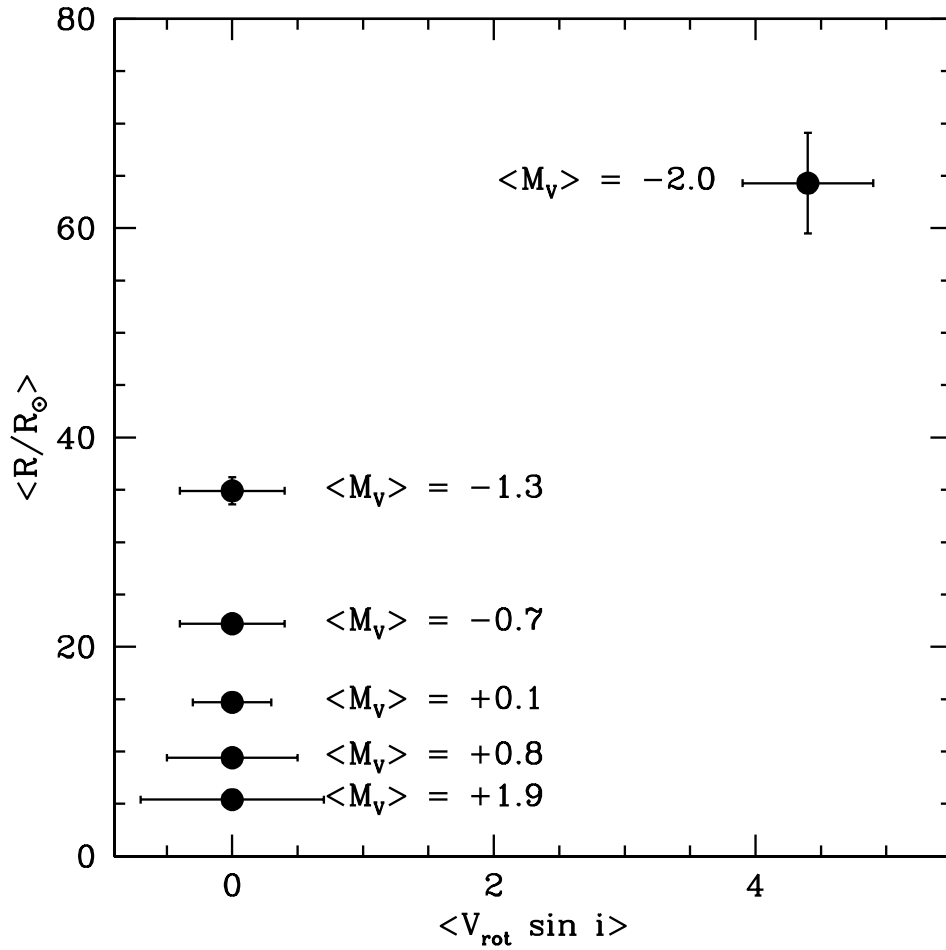


Fig. 14.— The binned results for stellar radii and stellar rotational values for metal-poor red giants from Table 5 are compared. For stars in five of the M_V bins, the estimated values of ζ_{RT} equal or exceed the average V_{broad} values, and the rotational velocities are set to zero. We show also the mean M_V values for each of the six bins. These results were computed by removing the effects of ζ_{RT} on total line broadening using Equation 1.

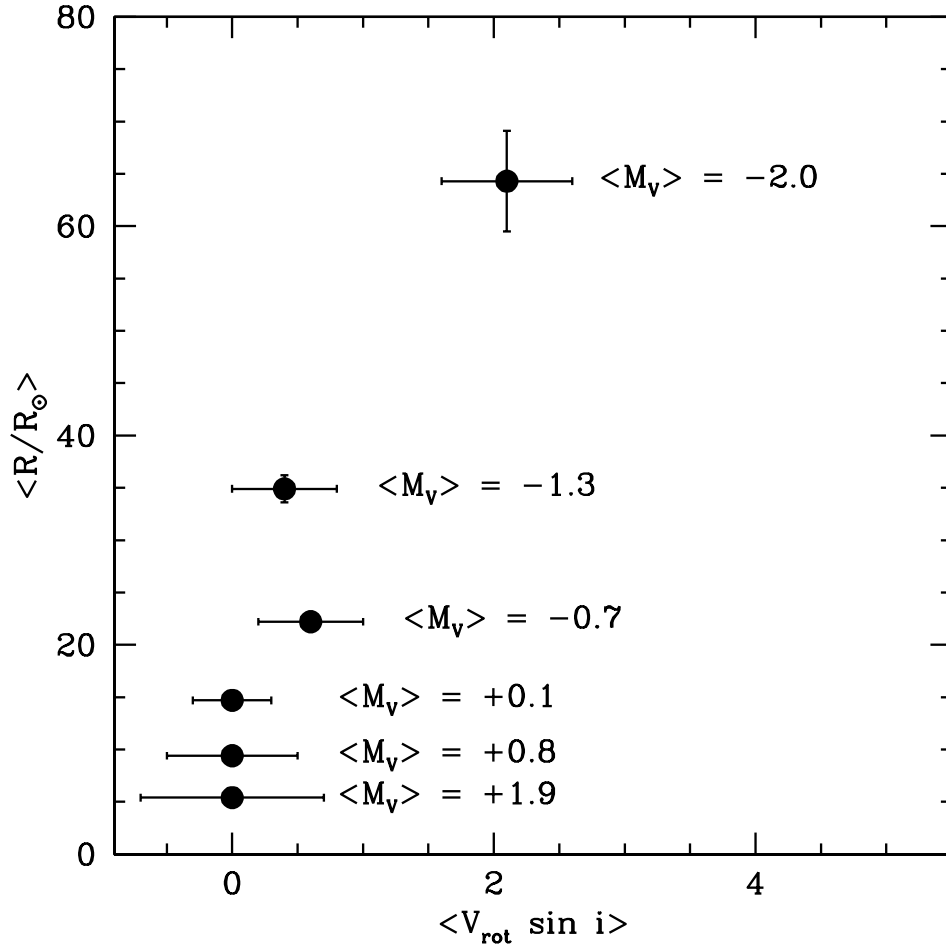


Fig. 15.— The binned results for stellar radii and stellar rotational values for metal-poor red giants from Table 5 are compared. For stars in five of the M_V bins, the estimated values of ζ_{RT} equal or exceed the average V_{broad} values, and the rotational velocities are set to zero. We show also the mean M_V values for each of the six bins. These results were computed using Equation 2, which does not make use of ζ_{RT} .

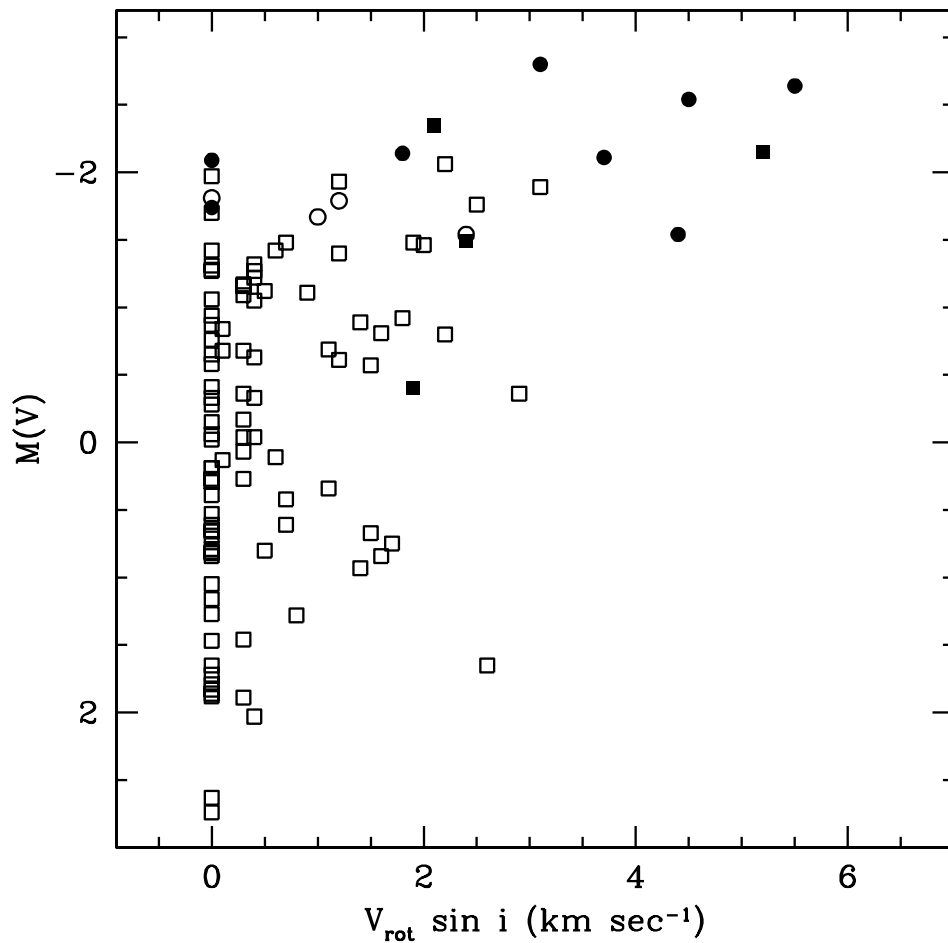


Fig. 16.— The individual results for stellar rotational velocities from Table 2 (circles) or use of Equation 2 (squares) are plotted against M_V . Filled circles and squares represent stars that display jitter, defined as $P(\chi^2) \leq 10^{-6}$, exclusive of orbital motion. Open circles and squares are stars that have not been found to manifest such random velocity variability.

